Title: Ankyrin-1 gene exhibits allelic heterogeneity in conferring protection against malaria

Author list and affiliations

Hong Ming Huang*, Denis C. Bauer[†], Patrick M. Lelliott[‡], Matthew W. A. Dixon[§], Leann Tilley[§], Brendan J. McMorran*, Simon J. Foote*, Gaetan Burgio*

*Department of Immunology and Infectious Disease, John Curtin School of Medical Research, Australian National University, ACT, Australia.

[†] CSIRO, Sydney, NSW, Australia.

[‡] IFReC Research Building, Osaka University, 3-1 Yamada-oka, Suita, Osaka 565-0871, Japan.

[§] Department of Biochemistry and Molecular Biology, Bio21 Institute, Melbourne, Victoria, Australia.

DOI: https://doi.org/10.1101/114959

Authors' Contributions

H.M.H., D.C.B., P.M.L., M.W.A.D, L.T., B.J.M, S.J.F. and G.B. designed and planned the experimental work. H.M.H., D.C.B. and G.B. performed the research. H.M.H., D.C.B., P.M.L., M.W.A.D, L.T., B.J.M, S.J.F. and G.B. interpreted and analysed the data. H.M.H., D.C.B. and G.B. performed statistical analysis. H.M.H, P.M.L., G.B., B.J.M. and S.J.F. wrote the manuscript. All authors reviewed the manuscript.

25 **Short Title: Allelic heterogeneity of Ankyrin-1**

26

27 **Keywords: Ankyrin-1, malaria, erythrocyte cytoskeleton, allelic heterogeneity**

28

29 **Corresponding author:**

30 Dr Gaetan Burgio

31 The John Curtin School of Medical Research, Australian National University,

32 131 Garran Road, ACT 2601, Australia.

33 Gaetan.burgio@anu.edu.au

34 +61 2 612 59428

35

Abstract

Allelic heterogeneity is a common phenomenon where a gene exhibit different phenotype depending on the nature of its genetic mutations. In the context of genes affecting malaria susceptibility, it allowed us to explore and understand the intricate host-parasite interactions during malaria infections. In this study, we described a gene encoding erythrocytic ankyrin-1 (*Ank-1*) which exhibits allelic-dependent heterogeneous phenotypes during malaria infections. We conducted an ENU mutagenesis screen on mice and identified two *Ank-1* mutations, one resulted in an amino acid substitution (MRI95845), and the other a truncated *Ank-1* protein (MRI96570). Both mutations caused hereditary spherocytosis-like phenotypes and confer differing protection against *Plasmodium chabaudi* infections. Upon further examination, the *Ank-1*$^{(MRI96570)}$ mutation was found to inhibit intra-erythrocytic parasite maturation, whereas *Ank-1*$^{(MRI95845)}$ caused increased bystander erythrocyte clearance during infection. This is the first description of allelic heterogeneity in ankyrin-1 from the direct comparison between two *Ank-1* mutations. Despite the lack of direct evidence from population studies, this data further supported the protective roles of ankyrin-1 mutations in conferring malaria protection. This study also emphasized the importance of such phenomenon to achieve a better understanding of host-parasite interactions, which could be the basis of future studies.

Introduction

Malarial parasites have been co-evolving with humans for thousands of years and have played a major role in shaping the human genome in malaria endemic regions [1,2]. Indeed, many genetic polymorphisms were selected for, as they provide significant host survival advantages during malaria infections [1,3], resulting in high frequencies of protective genetic mutations in malaria endemic regions. The majority of these affect the red blood cells (RBCs), and hence the blood stage of malaria infections [3-5].

Interestingly, these genetic mutations or alleles often exhibit varying degrees of malaria protection even if they affect the same gene, which is influenced by the location and the severity of the mutations [6,7]. This phenomenon, known as "allelic heterogeneity", is characterized by multiple different phenotypes arising from mutations in a single gene. It has been described for certain genes affecting malaria susceptibility, which is reflected by their geographical distribution within malaria-endemic regions [8]. One of the most prominent examples of this is the G6PD deficiency disorder, which can arise from multiple mutations in the G6PD gene [7,9]. Many studies have explored the effectiveness of each mutation in protecting individuals from malaria, which corresponds to the distribution of each allele across the globe [10-12]. Another example is the β-globin gene, which is well known for its two malaria protective alleles – the HbS and HbC in African populations [13,14]. HbC is restricted to West Africa, whereas HbS is widespread throughout Africa, which is thought to be linked to the effectiveness of each allele at conferring malaria resistance, and their non-malaria-associated morbidity [15,16]. Studies on these alleles would not only allow a better understanding of host-parasite interactions, but also give us insights into the dynamics of population genetics in malaria endemic regions [8].

79 However, allelic heterogeneity can also complicate the characterization of the malaria
80 protective roles of certain genes, often resulting in conflicting evidence from various studies.
81 One example of such polymorphisms is CD36 deficiency, which was originally thought to be
82 protective against malaria, as evidenced by the positive selection in East Asian and African
83 populations [17-19]. While some studies reported increased malaria protection [20], others
84 reported no significant associations [21] or even increased susceptibility [17,22]. It is
85 possible that these contradictive findings are due to confounding factors associated with
86 allelic heterogeneity in CD36 deficiency [6]. This further emphasizes the importance of
87 taking allelic heterogeneity into consideration better design future studies involving host
88 genetics in malaria, as well as various other infectious diseases.

89 In terms of malaria susceptibility, however, the allelic heterogeneity of genes affecting RBC
90 cytoskeleton is poorly understood. Many of the resulting genetic disorders are
91 heterogeneous, such as hereditary spherocytosis (HS), which is characterized by the
92 formation of "spherocytic" RBCs that exhibit reduced volume due to disruptions in
93 erythrocyte cytoskeletons. HS is caused by mutations in ankyrin, spectrins, band 3 and
94 protein 4.2, with ankyrin mutations contributing to more than 50% of all HS cases [23-27],
95 where the severity depends greatly on the location and the nature of mutations [28].
96 However, the prevalence of HS in malaria endemic regions is not well studied; only isolated
97 cases were reported [29-32]. Nevertheless, *in vivo* and *in vitro* studies have repeatedly
98 suggested an association of HS with increased malaria resistance, and several mechanisms
99 have been proposed, although not all of them were consistent [33-36]. Based on these
100 observations, we hypothesized that the inconsistencies in resistance mechanisms might be
101 due to the allelic heterogeneity of genes associated with HS.

102 To explore this hypothesis, we examined mouse models carrying two novel N-ethyl-N-
103 nitrosourea (ENU)-induced ankyrin mutations. These two mouse lines, *Ank-1*$^{(MRI96570/+)}$ and
104 *Ank-1*$^{(MRI95845/MRI95845)}$, displayed hematological and clinical features consistent with HS, and
105 a marked resistance to infection by the murine malarial parasite, *Plasmodium chabaudi*.
106 Analysis of the underlying mechanism of resistance to infection revealed both common and
107 distinct features between the strains. RBCs from both mouse lines were similarly resistant
108 to merozoite invasion. Although, the *Ank-1*$^{(MRI95845/MRI95845)}$ erythrocytes were more rapidly
109 cleared from circulation during an infection, an impairment in intra-erythrocytic parasite
110 maturation was observed in the infected *Ank-1*$^{(MRI96570/+)}$ erythrocytes. This study highlights
111 the first direct examination of allelic heterogeneity of the *Ank-1* gene in the context of
112 malaria resistance in mouse models.

113

114

115 **Materials and Methods**

116 *Mice and ethics statement*

117 All mice used in this study were housed with 12 hour light-dark cycle under constant
118 temperature at 21 °C, with food and water available *ad libitum*. All procedures were
119 performed according to the National Health and Medical Research Council (NHMRC)
120 Australian code of practice. Experiments were carried out under ethics agreement AEEC
121 A2014/54, which was approved by the animal ethics committees of the Australian National
122 University.

123

124 *ENU mutagenesis and dominant phenotype screening*

125 SJL/J male mice were injected intraperitoneally with two doses of 100 mg/kg ENU (Sigma-
126 Aldrich, St Louis, MO) at one week interval. The treated males (G0) were crossed to females
127 from the isogenic background to produce the first generation progeny (G1). The seven-
128 week-old G1 progeny were bled and analyzed on an Advia 120 Automated Hematology
129 Analyzer (Siemens, Berlin, Germany) to identify abnormal red blood cell count. A mouse
130 carrying the MRI96570 or MRI95845 mutation was identified with a RBC "mean corpuscular
131 volume" (MCV) value three standard deviations lower from other G1 progeny. It was
132 crossed with SJL/J mice to produce G2 progeny to test the heritability of the mutations and
133 the dominance mode of inheritance. Mice that exhibited low MCV (<48fL) were selected for
134 whole exome sequencing and genotyping.

135

136 *Whole exome sequencing*

137 DNA from two G2 mice per strain carrying the abnormal red blood cell parameters (MCV
138 <48fL) were extracted with Qiagen DNeasy blood and tissue kit (Qiagen, Venlo, Netherlands)
139 for exome sequencing as previously described [37]. Briefly, 10µg of DNA was prepared for
140 exome enrichment with Agilent Sure select kit paired-end genomic library from Illumina
141 (San Diego, CA), followed by high throughput sequencing using a HiSeq 2000 platform. The
142 bioinformatics analysis was conducted according to the variant filtering method previously
143 described by Bauer et al. [38]. Private variants that were shared between the two mutants
144 but not with other SJL/J, C57BL/6 mice, excluding the common variants between other
145 mouse strains were annotated using ANNOVAR [39]. Private non-synonymous exonic and

146 intronic variants within 20 bp from the exon spicing sites were retained as potential
147 candidate ENU mutations.

148

149 *PCR and Sanger sequencing*

150 DNA from mutant mice was amplified through PCR with 35 cycles of 30 seconds of 95^0C
151 denaturation, 30 seconds of 56-58^0C annealing and 72^0C elongation for 40 seconds. The
152 primers used in the PCR are described below. The PCR products were examined with
153 agarose gel electrophoresis before being sent to the Australian Genome Research Facility
154 (AGRF) in Melbourne, Australia, for Sanger sequencing. Logarithm of odds (LOD) score was
155 calculated based on the number of mice that segregated with the candidate mutations.

156 Primers for MRI95845 mutation:

Amplicon	Forward	Reverse
Snai2	CATCTGCAGACCCACTCTGA	TGGTTGGTAAGCACATGAGAA
Tbc1d23	CACCCCCTTTTTGGTTTCTT	ACGTGCACATCGACTAACCA
Pnpla6	AGGCTGAGGAAGTGTGCCTA	AACTAGCTGGGCTTTGGTCA
Zglp1	CTGGCCTTTGACTTCTGACC	CCTCACAAGGTGGCTGTTTC
Ank-1	CTCCAAGTGAGAGGGTTTGC	GATGGCACACAGTCAGACCA

157

158 Primers for MRI96570 mutation:

Amplicon	Forward	Reverse
Fat4	CGCATCCCTTCATACAACCT	ACACCCCACTCACGTAGCTC
Rhcg	TGAGGAATGAGGGAGAAAGG	CCAATATGGCAGCCCTCTAA
Plxnb3	TACCCGATCAATCCAGAAGG	TTCTGAATGTGCAGGGTCAC
Ank-1	TGTGCAGGCATTTCTACATGA	ACTCTCTGGGTAGACCCCGT

159

160

161 *RBC osmotic fragility analysis*

162 To assess the susceptibility of RBC membrane to osmotic stress, 5µl of mouse whole blood
163 was diluted 100-fold with phosphate buffer (pH 7.4) containing 0 to 10g/L of sodium
164 chloride, and incubated for at least 10 minutes at room temperature. The cells were
165 centrifuged at 800g for 3 minutes, and the supernatant, which contains free hemoglobin,
166 was measured at 540nm to assess the degree of hemolysis. The absorbance values were
167 expressed as percentage of hemolysis, with hemolysis at 0g/L sodium considered as 100%
168 lysis.

169

170 *Erythrocyte lifetime assay*

171 Each uninfected mouse was intravenously injected with 1mg of EZ-link® Sulfo-NHS- LC Biotin
172 (Biotin) (Thermo Scientific, Waltham, MA) in mouse tonicity PBS (MT-PBS). 2ul of blood was
173 collected on day 1, 7, 14, 21 and 28 days post-injection. Samples were stained and analyzed
174 using a flow cytometer. The proportion of Biotin-labelled mature RBCs on day 1 was
175 considered as the "starting point" of 100% of labelled cells. For subsequent timepoints, the
176 remaining number of biotin-labelled RBCs were expressed as a percentage of the starting
177 number as the indication of RBC turnover rate.

178 For infected mice, 1mg of Biotin was injected intravenously as soon as parasitemia was
179 detectable via flow cytometry (approximately 0.05-0.3%). Samples were collected daily and
180 analyzed as above.

181

182 *Ektacytometry*

183 10-15ul of uninfected RBCs were first resuspended in 500ul of pre-warmed
184 polyvinylpyrrolidone (PVP) solution at a viscosity of 30 mPa/second at 37 °C until needed.
185 Samples were analyzed according to the manufacturer's instructions with a RheoScan
186 Ektacytometer (Rheo Meditech, Seoul, South Korea) and the elongation index measured
187 across a range of pressures from 0-20 Pa. Each sample was measured three times to account
188 for technical variabilities. The values were normalized against the wild-type samples.

189

190 *In vitro spleen retention assay*

191 The RBC deformability was examined according to the protocol described previous by
192 Deplaine et al. [40] with modifications. Briefly, RBCs from each genotype of mice were
193 stained with 10µg/ml of either hydroxysulfosuccinimide Atto 633 (Atto 633) or
194 hydroxysulfosuccinimide Atto 565 (Atto 565) (Sigma-Aldrich, St Louis, MO), followed by
195 three washes with MTRC (154mM NaCl, 5.6mM KCl, 1mM $MgCl_2$, 2.2mM $CaCl_2$, 20mM
196 HEPES, 10mM glucose, 4mM EDTA, 0.5% BSA, pH 7.4, filter sterilized). The stained RBCs
197 were mixed in equal proportion and diluted with unstained wild-type RBCs to give
198 approximately 10-20% of the total RBCs being labelled RBCs. The samples were further
199 diluted to 1-2% haematocrit with MTRC, before passing through the filter bed. The pre-
200 filtered and post-filtered samples were analysed on BD LSRFortessa (BD Biosciences,
201 Franklin Lakes, NJ) flow cytometer to determine the proportion being retained in the filter
202 bed.

203

204 *Scanning electron microscopy (SEM)*

205 SEM was performed as described previously [41]. Mouse blood was fixed overnight in 3%
206 EM-grade glutaraldehyde (Sigma-Aldrich, St Louis, MO) at 4°C immediately upon collection.
207 The samples were washed with MT-PBS 3 times, 10 minute each time. The cells were then
208 adhered to the coverslips with 0.1% polyethylenimine (PEI) for 10 minutes, before washing
209 with MT-PBS. The cells were then dried serially using 30%, 50%, 70%, 80%, 90%, 100%, 100%
210 ethanol, 10 minutes each. The cells were then soaked in 1:1 ethanol: hexamethyldisilazane
211 solution for 10 minutes, followed by 2 washes with 100% hexamethyldisilazane (Sigma-
212 Aldrich, St Louis, MO), each 10 minutes. The coverslips were then air-dried overnight and
213 coated with gold and examined under JEOL JSM-6480LV scanning electron microscope.

214

215 *Quantitative PCR and cDNA sequencing*

216 RNA was purified from embryonic livers of E14 embryos using Qiagen RNeasy kit (Qiagen,
217 Venlo, Netherlands), followed by cDNA synthesis using Transcriptor High Fidelity cDNA
218 Synthesis Kit (Roche, Basel, Switzerland), as described previously [41]. Quantitative PCR was
219 performed on ViiA™ 7 Real-Time PCR System (Thermo Scientific, Waltham, MA). The $\Delta\Delta C_T$
220 method [42] was used to determine the cDNA levels of *Ank-1* and the housekeeping gene β-
221 actin and expressed as a fold-change of the mutants to the wild-type. The primers used for
222 *Ank-1* gene spanned exon 2 to 4: *Ank-1*-F: 5'-TAACCAGAACGGGTTGAACG-3'; *Ank-1*-R: 5'-
223 TGTTCCCCTTCTTGGTTGTC-3'; β-Actin-F: 5'- TTCTTTGCAGCTCCTTCGTTGCCG-3'; β-Actin-R: 5'-
224 TGGATGCGTACGTACATGGCTGGG-3'.

225

226 *SDS-PAGE, Coomassie staining and Western blot*

227 The analysis of erythrocytic proteins was carried out as described previously [41]. Briefly,
228 RBC ghosts were prepared by lysing mouse RBCs with ice-cold 5mM phosphate buffer
229 (ph7.4) and centrifuging at 20,000g for 20 minutes followed by removal of the supernatant,
230 and repeat until the supernatant became clear. The RBC ghosts or whole blood lysates were
231 denatured in SDS-PAGE loading buffer (0.0625M Tris pH 6.8, 2% SDS, 10% glycerol, 0.1M
232 DTT, 0.01% bromophenol blue) at 95°C for 5 minutes before loading onto a 4-15% Mini-
233 PROTEAN® TGX™ Precast Gels (Bio-Rad, Hercules, CA). The gels were then either stained
234 with Coomassie blue solution (45% v/v methanol, 7% v/v acetic acid, 0.25% w/v Brilliant
235 Blue G) overnight or transferred to a nitrocellulose membrane. The western blot was carried
236 out using these primary antibodies: 1ug/ml anti-alpha 1 spectrin (clone 17C7), 1ug/ml anti-
237 beta 1 spectrin (clone 4C3) (Abcam, Cambridge, UK), 0.5ug/ml anti-GAPDH (clone 6C5)
238 (Merck Millipore, Darmstadt, Germany), anti-N-terminal *Ank-1* "p89" at 1:1500 dilution,
239 anti-band 3 at 1:4000 dilution and anti-protein 4.2 at 1:2000 dilution (kind gifts from Connie
240 Birkenmeier, Jackson Laboratory, US). Each primary antibody was detected with the
241 appropriate horseradish peroxidase (HRP)-conjugated secondary antibody at 1:5000 dilution
242 from 1mg/ml stocks. The blots were visualized using ImageQuant LAS 4000 (GE Healthcare
243 Life Sciences, Arlington Heights, IL), and quantified using ImageJ software [43].

244

245 *Malaria infection*

246 Malaria infections on mice were performed as described previously [41]. 200µl of thawed *P.*
247 *chabaudi adami* infected blood was injected into the intraperitoneal cavity of a C57BL/6
248 donor mouse. When the donor mouse reached 1-10% parasite load (parasitemia), blood was
249 collected through cardiac puncture. The blood was diluted with Krebs' buffered saline with

250 0.2% glucose as described previously [44]. Each experimental mouse was infected with
251 $1x10^4$ parasites intraperitoneally. The parasitemia of these mice were monitored either
252 using light microscopy or flow cytometry.

253

254 *Terminal deoxynucleotidyl transferase dUTP nick end labelling (TUNEL) staining*

255 The TUNEL assay was carried out as described previously [41] with slight modification. 3µl of
256 infected blood containing 1-10% parasitemia were collected during trophozoite stage and
257 fixed in 1 in 4 diluted BD Cytofix™ Fixation Buffer (BD Biosciences, Franklin Lakes, NJ) for at
258 least day until they were needed. Each sample was then washed twice with MT-PBS, and
259 adhered to a glass slide pre-coated with 0.1% polyethylenimine (PEI) for 10 minutes at room
260 temperature. The excess cells were washed and the glass slide was incubated overnight at
261 room temperature with TUNEL labelling solution (1mM Cobalt Chloride, 25mM Tris-HCl pH
262 6.6, 200mM sodium cacodylate, 0.25mg/ml BSA, 60uM BrdUTP, 15U Terminal transferase).
263 The slides were washed three times, followed by staining with 50µg/ml of anti-BrdU-FITC
264 antibody (Novus Biologicals, Littleton, CO) in MT-PBT (MT-PBS, 0.5% BSA, 0.05% Triton X-
265 100) for 1 hour. The slides were then washed three times with MT-PBS and mounted with
266 SlowFade® Gold antifade reagent with DAPI (Thermo Scientific, Waltham, MA) and sealed.
267 When the slides were dried, they were examined using Axioplan 2 fluorescence light
268 microscope (Carl Zeiss, Oberkochen, Germany) between 60x to 100x magnification. At least
269 100 DAPI-positive cells were counted, and each was graded as either positive or negative for
270 TUNEL staining, as an indication of DNA fragmentation.

271

272 *In vivo erythrocyte tracking (IVET) assays*

273 The IVET assay was carried out as previously described by Lelliott et al. [45],[46]. Briefly, at
274 least 1.5ml whole blood was collected from mice of each genotype via cardiac puncture,
275 followed by staining with either 10µg/ml of Atto 633 or 125µg/ml of EZ-Link™ Sulfo-NHS-LC-
276 Biotin (Biotin) (Thermo Scientific, Waltham, MA) for 45 minutes at room temperature,
277 followed by washing two times with MT-PBS. The blood was mixed in two different dye
278 combinations to correct for any dye effects. Approximately $1x10^9$ erythrocytes were injected
279 intravenously into infected wild-type mice at 1-5% parasitemia during schizogony stage.
280 Blood samples were collected at various timepoints, from 30 minutes up to 36 hours after
281 injection, and analyzed using flow cytometry. The ratio of infected labelled erythrocytes was
282 determined, as an indication of the relative susceptibility of RBCs to *P. chabaudi* infections.
283 The proportion of labelled blood populations was also tracked over time to determine the
284 clearance of these RBCs from the circulation.

285

286 *Flow cytometry analysis of blood samples*

287 For erythrocyte lifetime assays, 2µl of whole blood samples were stained with 2µg/ml
288 streptavidin-PE-Cy7, 1µg/ml anti-CD71-allophycocyanin (APC) (clone R17217), 1µg/ml anti-
289 CD45–APC eFluor 780 (clone 30-F11) (eBioscience, San Diego, CA), 4µM Hoechst 33342
290 (Sigma-Aldrich, St Louis, MO) and 12µM JC-1 (Thermo Scientific, Waltham, MA) in MTRC.
291 The samples were washed once with MTRC and further stained with 2µg/ml streptavidin-PE-
292 Cy7 to capture all biotin-labelled cells. Immediately prior to analyzing on flow cytometer, 5µl
293 of 123count eBeads (eBioscience, San Diego, CA) was added to determine the relative levels
294 of anemia.

295 For both malaria infections and IVET assay, 2µl of whole blood samples were stained with
296 2µg/ml streptavidin-PE-Cy7 (only for experiments with biotinylated erythrocytes), 1µg/ml
297 anti-CD45–allophycocyanin (APC)–eFluor 780 (clone 30-F11), 1µg/ml anti-CD71 (TFR1)–
298 PerCP–eFluor 710 (clone R17217) (eBioscience, San Diego, CA), 4µM Hoechst 33342 (Sigma-
299 Aldrich, St Louis, MO) and 12µM JC-1 (Thermo Scientific, Waltham, MA) in MTRC. All
300 samples analyzed through flow cytometry were performed on BD LSRFortessa (BD
301 Biosciences, Franklin Lakes, NJ), where 200,000 to 1,000,000 events were collected and
302 visualized on FACSDiva™ and FlowJo software. RBCs were identified by gating on CD71
303 negative and CD45 negative population, followed by gating on Atto-labelled and Biotin-
304 labelled erythrocytes on appropriate channels (APC for Atto-633, PE for Atto-565 and PE-
305 Cy7 for Biotin). The parasitemia of each labelled erythrocyte population was determined by
306 gating on Hoechst 33342 positive and JC-1 positive population.

307

308 *Statistical analysis*

309 The statistical analysis was carried out as described in previous study [41]. Unless otherwise
310 stated, all statistical analysis was carried out using unpaired two-tailed Student's t-tests
311 without corrections. In particular, the LOD score method coupled with Bonferroni correction
312 was used to determine the causative mutation for MRI96570 and MRI95845, in which the
313 significance threshold and the LOD score for each candidate mutation was calculated, and a
314 LOD score above the threshold was considered statistically significant. The statistical tests
315 for FRAP assay, ektacytometry, RBC lifetime and clearance assays were performed by first
316 calculating the area under curves for each sample, followed by an unpaired Student's t-test
317 on pooled mice of each genotype. The statistical tests for *in vitro* spleen retention assays

318 were performed using paired Sudent's t-test, comparing mutant with wild-type RBC
319 population within the same sample. The statistical significance of the malaria survival was
320 tested using the unpaired Log-Rank test on pooled mutant versus wild-type mice. The
321 statistical significance of *Plasmodium* infection was determined via the statmod software
322 package for R (http://bioinf.wehi.edu.au/software/compareCurves) using the
323 'compareGrowthCurves' function with 10,000 permutation, followed by adjustments for
324 multiple testing. The statistical significance for the ratios of IVET assays was determined
325 using the one sample t-test with hypothetical mean of 1.

326

327 **Results**

328 **MRI96570 and MRI95845 carry mutations in *Ank-1* gene**

329 ENU-treated SJL/J male mice were crossed with wild-type female to produce G1 progeny.
330 The G1 progeny carrying heterozygous point mutations in their genome were then
331 subjected to hematological screening to identify genes affecting RBC properties that might
332 confer malaria protection. Heterozygous G1 mice MRI96570 and MRI95845 were identified
333 from the ENU-dominant screen with mean cellular volume (MCV) three standard deviations
334 below the normal level of the respective parental line: 48.5fl for MRI96570, and 50.6fl for
335 MRI95845, compared to the background of 55.1±1.2fl in SJL/J inbred strain. These mice
336 were crossed with wild-type to produce G2 progeny, where approximately half exhibit low
337 erythrocyte MCV values. Exome sequencing was carried out from two MRI96570 and
338 MRI95845 G2 progeny showing a reduction of MCV to identify the causative genetic
339 mutations. Unique variants shared between these mice were identified and listed in Table
340 S1. A mutation in the ankyrin-1 (*Ank-1*) gene was present in all the affected mice, and co-

341 segregated completely with the reduced MCV phenotype for over three generations of
342 crosses. Sanger sequencing revealed a T to A transversion in exon 34 of the *Ank-1* gene for
343 MRI96570 strain, and a T to A transversion in exon 5 of the *Ank-1* gene for MRI95845 strain
344 (Figure S1). They were predicted to cause a nonsense mutation at amino acid position 1398,
345 located in the spectrin-binding domain for MRI96570 mice, and a substitution of tyrosine for
346 asparagine at amino acid residue 149 in the 4th ankyrin repeat for MRI95845 mice (Figure
347 1A). MRI96570 and MRI95845 will be referred as *Ank-1*$^{(MRI96570)}$ and *Ank-1*$^{(MRI95845)}$
348 respectively, for the rest of the report.

349

350 **Both *Ank-1*$^{(MRI96570)}$ and *Ank-1*$^{(MRI95845)}$ exhibit HS-like phenotypes**

351 Since ankyrin mutations are usually associated with HS, we examined both *Ank-1*$^{(MRI96570)}$
352 and *Ank-1*$^{(MRI95845)}$ mice in terms of their HS-like phenotypes. When two *Ank-1*$^{(MRI96570/+)}$ G2
353 progeny were intercrossed, *Ank-1*$^{(MRI96570/MRI96570)}$ mice were born with severe jaundice and
354 died within several days of birth (Figure 1B), suggesting homozygosity for *Ank-1*$^{(MRI96570)}$
355 mutation caused lethal anemia. On the other hand, *Ank-1*$^{(MRI95845/MRI95845)}$ mice appeared
356 healthy with a normal lifespan. Hematological analysis of these mice revealed a significant
357 reduction in MCV and mean corpuscular hemoglobin (MCH), and increased red cell
358 distribution width (RDW) (Table S2), indicating microcytosis and anisocytosis, which are the
359 hallmarks for HS. When the RBCs were subjected to osmotic stress, RBCs from *Ank-*
360 *1*$^{(MRI96570/+)}$, *Ank-1*$^{(MRI95845/+)}$ and *Ank-1*$^{(MRI95845/MRI95845)}$ mice exhibit significantly increased
361 osmotic fragility compared to wild-type RBCs (Figure 1C). In particular, sodium chloride
362 concentration required to achieve 50% hemolysis is significantly higher ($P<0.001$) for *Ank-*
363 *1*$^{(MRI96570/+)}$ RBCs (5.6 g/L or 104mM) and *Ank-1*$^{(MRI95845/+)}$ RBCs (5.4 g/L or 100mM),

364 compared to wild-type RBCs (4.6 g/L or 84mM). The *Ank-1*$^{(MRI95845/MRI95845)}$ RBCs showed
365 further susceptibility to osmotic stress, with 50% hemolysis at approximately 6.5 g/L
366 (121mM) sodium chloride concentration.

367

368 We predicted that the mutant RBCs have shorter half-life, which is also one of the
369 symptoms of HS. Therefore, RBC half-life was determined by biotinylating mouse RBCs *in*
370 *situ* and tracking the proportion of biotinylated RBCs in circulation over time. As shown in
371 Figure 1D, erythrocytes from *Ank-1*$^{(MRI95845/MRI95845)}$ have a significantly shorter half-life of
372 approximately 9.5 days as opposed to the 16 days of wild-type erythrocytes (P=0.008), but
373 no significant difference was observed for erythrocytes from heterozygous mice (P=0.09 for
374 *Ank-1*$^{(MRI96570/+)}$ mice and P=0.08 for *Ank-1*$^{(MRI95845/+)}$ mice). The morphology of these RBCs
375 were examined under light and scanning electron microscopy (Figure S2). *Ank-1*$^{(MRI96570/+)}$
376 and *Ank-1*$^{(MRI95845/+)}$ mice exhibited slight reduction in RBC size, while *Ank-1*$^{(MRI95845/MRI95845)}$
377 mice had smaller acanthocytic RBCs and displayed anisocytosis. On the other hand, blood
378 smears obtained from jaundiced *Ank-1*$^{(MRI96570/MRI96570)}$ pups showed reticulocytosis,
379 fragmented RBCs and severe anisocytosis.

380 Another feature of HS is reduced RBC deformability, which was examined using two
381 different analytical techniques: ektacytometry and an *in vitro* spleen retention assay.
382 Ektacytometry measures the flexibility of RBCs when subjected to shear pressure, and
383 expresses as an elongation index, which indicates the deformability of RBCs. The *Ank-*
384 *1*$^{(MRI96570/+)}$ RBCs showed reduced elongation index compared to wild-type, with *Ank-*
385 *1*$^{(MRI95845/MRI95845)}$ RBCs showing further reduction in elongation index, indicating significant
386 reduction in RBC deformability (Figure 1E). In addition, the *in vitro* "spleen mimic" retention

387 assay was performed by passing the erythrocytes through layer of microbeads of varying
388 sizes, modelling *in vivo* splenic filtration. RBC deformability was assessed by the ability of
389 RBCs to pass through the bead layer. Figure 1F showed three independent measurements of
390 RBC deformability using the splenic retention assay, comparing wild-type, *Ank-1*$^{(MRI96570/+)}$,
391 *Ank-1*$^{(MRI95845/+)}$ and *Ank-1*$^{(MRI95845/MRI95845)}$ RBCs. An approximately 70% increased retention
392 for *Ank-1*$^{(MRI96570/+)}$ RBCs was observed compared to wild-type, whereas erythrocytes of *Ank-*
393 *1*$^{(MRI95845/+)}$ and *Ank-1*$^{(MRI95845/MRI95845)}$ mice showed 86% and 90% increased RBC retention
394 compared to wild-type, respectively. However, no significant difference was observed
395 between *Ank-1*$^{(MRI96570/+)}$ and *Ank-1*$^{(MRI95845/MRI95845)}$ erythrocytes.

396 The expression levels of ankyrin and other RBC membrane proteins were also examined
397 (Figure S3). Significant reduction of *Ank-1* mRNA levels was observed in *Ank-1*$^{(MRI96570/+)}$,
398 *Ank-1*$^{(MRI95845/+)}$, *Ank-1*$^{(MRI96570/MRI96570)}$ and *Ank-1*$^{(MRI95845/MRI95845)}$ embryonic livers (Figure
399 S3a). However, Coomassie staining and Western blotting of the RBC membrane fractions did
400 not show a significant difference in ANK-1 levels between wild-type, *Ank-1*$^{(MRI96570/+)}$ and
401 *Ank-1*$^{(MRI95845/MRI95845)}$ erythrocytes (P=0.3) (Figure S3b-d), using an anti-ANK-1 antibody (p89)
402 targeting specifically to the N-terminal region of ANK-1 protein [36]. The predicted
403 truncated ANK-1$^{(MRI96570/+)}$ form (160kDa) was also not evidenced, suggesting degradation of
404 truncated protein. The levels of other cytoskeletal proteins were also examined to account
405 for possible disruptions to interactions with binding partners of ankyrin-1. However, no
406 difference was observed for band 3, α- and β-spectrin, whereas with a significantly lower
407 protein 4.2 level was observed only in *Ank-1*$^{(MRI95845/MRI95845)}$ erythrocytes (Figure S3d).

408

409 **_Ank-1_$^{(MRI96570)}$ and _Ank-1_$^{(MRI95845)}$ confer protection against _P. chabaudi_ infection**

410 We proposed that mice carrying these mutations have reduced susceptibility to malaria
411 infection, which we examined by injecting with a lethal dose of *P. chabaudi*, and recording
412 the percentage of parasitized RBCs (parasitemia). As shown in Figure 2A, *Ank-1*$^{(MRI96570/+)}$ and
413 *Ank-1*$^{(MRI95845/+)}$ mice showed significant reduction in peak parasitemia of approximately 15-
414 20%, while *Ank-1*$^{(MRI95845/MRI95845)}$ mice showed approximately 30% reduction in peak
415 parasitemia compared to wild-type. *Ank-1*$^{(MRI95845/MRI95845)}$ mice also showed a two-day delay
416 in parasitemia, peaking on day 12 post-infection rather than day 10 as with wild-type. *Ank-*
417 *1*$^{(MRI95845/MRI95845)}$ mice also exhibited significantly higher survival rate compared to wild-type
418 during *P. chabaudi* infection, but no significant difference was observed for *Ank-1*$^{(MRI96570/+)}$
419 and *Ank-1*$^{(MRI95845/+)}$ mice compared to wild-type (Figure 2B). Overall, these results suggested
420 that both *Ank-1*$^{(MRI96570/+)}$ and *Ank-1*$^{(MRI95845/+)}$ mice showed moderate resistance, whereas
421 *Ank-1*$^{(MRI95845/MRI95845)}$ mice exhibited significant resistance towards *P. chabaudi* infection
422 relative to wild-type mice.

423 From these results, we further investigated and compared the possible mechanisms of
424 resistance mediated by *Ank-1*$^{(MRI96570)}$ and *Ank-1*$^{(MRI95845)}$ mutations. We examined three
425 important determinants of parasite growth and survival within the host. Firstly, we studied
426 the ability of parasite to survive within these erythrocytes, since ankyrin-1 mutations have
427 previously been implicated to impair parasite intra-erythrocytic maturation [36]. Secondly,
428 the erythrocyte invasion was assessed since the mutations disrupt erythrocyte cytoskeletal
429 structure, which is important for facilitating efficient erythrocyte invasion [47]. Thirdly, the
430 mutations might result in an improved detection of parasitized RBCs, thus enhancing their
431 removal from circulation during malaria infection. Since *Ank-1*$^{(MRI96570/+)}$ and *Ank-*
432 *1*$^{(MRI95845/MRI95845)}$ mice exhibited differences in malaria resistance, we hypothesized that they
433 mediate malaria resistance through different pathways.

434

435 ***Ank-1*$^{(MRI96570/+)}$ and *Ank-1*$^{(MRI95845/MRI95845)}$ erythrocytes are resistant to merozoite invasion**

436 First, the ability of parasites to invade erythrocytes was assessed via an *in vivo* erythrocyte
437 tracking (IVET) assay. Labelled RBCs from either wild-type, *Ank-1*$^{(MRI96570/+)}$ or *Ank-*
438 *1*$^{(MRI95845/MRI95845)}$ mice were injected into infected wild-type mice of 1-10% parasitemia
439 during late schizogony stage and the parasitemia of each genotype was monitored over 36-
440 40 hours to indicate relative invasion rates. The initial invasion period was expected at 30
441 minutes to 3 hours post-injection, and the results were expressed as a ratio of parasitized
442 RBCs of either, *Ank-1*$^{(MRI96570/+)}$ to wild-type (Figure 3A), *Ank-1*$^{(MRI95845/MRI95845)}$ to wild-type
443 (Figure 3B), or *Ank-1*$^{(MRI96570/+)}$ to *Ank-1*$^{(MRI95845/MRI95845)}$ (Figure 3C). From Figure 3A and 3B,
444 *Ank-1*$^{(MRI96570/+)}$ and *Ank-1*$^{(MRI95845/MRI95845)}$ erythrocytes were less parasitized compared to
445 wild-type (0.6-0.7 for *Ank-1*$^{(MRI96570/+)}$ to wild-type, $P<0.001$; and 0.55-0.8 for *Ank-*
446 *1*$^{(MRI95845/MRI95845)}$ to wildtype, $P<0.001$) from 3 hours up to 36 hours post-injection, indicating
447 both *Ank-1*$^{(MRI96570/+)}$ and *Ank-1*$^{(MRI95845/MRI95845)}$ erythrocytes were more resistant to parasite
448 invasion than wild-type. However, no significant differences in parasitemia ratio were
449 observed at the 30 minute timepoint. Furthermore, when the invasion rate of both *Ank-*
450 *1*$^{(MRI96570/+)}$ and *Ank-1*$^{(MRI95845/MRI95845)}$ erythrocytes were compared in infected wild-type mice
451 (Figure 3C), no significant difference in parasitemia ratio was observed, suggesting a similar
452 invasion rate between the two mutant erythrocytes.

453

454 ***Ank-1*$^{(MRI96570/+)}$ erythrocytes impair parasite maturation**

455 Second, the parasite intra-erythrocytic maturation was determined through a TUNEL assay,
456 which allows the detection of fragmented DNA in RBCs, as an indication of dying parasites
457 (Figure 3D) [48]. Samples were collected from infected mice at 1-10% parasitemia at both
458 young ring stage and late trophozoite stage, and the proportion of TUNEL-positive infected
459 RBCs were measured. As seen from Figure 3E, more TUNEL-positive parasites were observed
460 within *Ank-1*$^{(MRI96570/+)}$ erythrocytes, in both ring (30.1±3.4% compared to 15.2±3.1% of wild-
461 type) and trophozoite stage (30.8±3.8% compared to 11.7±1.0% of wild-type), whereas no
462 differences were observed for *Ank-1*$^{(MRI95845/+)}$ and *Ank-1*$^{(MRI95845/MRI95845)}$ erythrocytes. This
463 result suggested that the growth of parasites within *Ank-1*$^{(MRI96570/+)}$ erythrocytes was
464 impaired, but was normal in *Ank-1*$^{(MRI95845/+)}$ and *Ank-1*$^{(MRI95845/MRI95845)}$ erythrocytes. This
465 also indicate that *Ank-1*$^{(MRI96570)}$ disrupts parasite maturation, whereas *Ank-1*$^{(MRI95845)}$ seems
466 to support normal parasite growth.

467

468 ***Ank-1*$^{(MRI95845/MRI95845)}$ erythrocytes are more likely to get cleared during malaria infections,**
469 **partially via splenic filtration**

470 The proportions of labelled erythrocytes were also monitored during the IVET assays to
471 compare the relative loss of the two labelled RBC populations as an indicator of RBC
472 clearance during malaria infection. No significant reduction in *Ank-1*$^{(MRI96570/+)}$ erythrocyte
473 numbers was observed during IVET assay compared to wild-type (Figure 4A). In contrast, the
474 number of labelled *Ank-1*$^{(MRI95845/MRI95845)}$ erythrocytes decreased significantly compared to
475 wild-type and *Ank-1*$^{(MRI96570/+)}$ erythrocytes (Figure 4B and C), with approximately 20% and
476 50% reduction, respectively. However, the parasitemia measurements during the IVET
477 assays were approximately 2% to 16-30% (Figure S4a-b), which did not correlate with the

478 reduction of labelled *Ank-1*$^{(MRI95845/MRI95845)}$ erythrocytes. This suggested an increased
479 bystander clearance rather than clearance of infected *Ank-1*$^{(MRI95845/MRI95845)}$ RBCs. To further
480 verify this observation, the infected mice from each genotype were injected with biotin and
481 the biotinylated RBC half-life was examined. As shown in Figure 4D, the *Ank-1*$^{(MRI96570/+)}$ mice
482 exhibited no significant reduction in RBC numbers, whereas *Ank-1*$^{(MRI95845/MRI95845)}$ mice were
483 found to have significantly shorter half-life of approximately 6 days, which did not correlate
484 with the parasitemia curve (Figure S4c). This observation of shorter RBC half-life in infected
485 *Ank-1*$^{(MRI95845/MRI95845)}$ mice is consistent with the increased *Ank-1*$^{(MRI95845/MRI95845)}$ erythrocyte
486 clearance as shown in IVET assays.

487 We proposed that the spleen played a major role in mediating this bystander clearance.
488 Therefore, we infected splenectomized mice with *P. chabaudi* and infused with labelled
489 wild-type and *Ank-1*$^{(MRI95845/MRI95845)}$ erythrocytes, the proportions of which were monitored
490 over time. As shown in Figure 4E, *Ank-1*$^{(MRI95845/MRI95845)}$ erythrocyte numbers are
491 approximately two-fold higher ($P<0.01$) in splenectomized mice compared to non-
492 splenectomized mice. This suggests that the spleen is a major contributor towards *Ank-*
493 *1*$^{(MRI95845/MRI95845)}$ erythrocyte clearance, although the clearance was not completely
494 abrogated in the absence of the spleen.

495

496 **Increased Band 3 mobility in *Ank-1*$^{(MRI95845/MRI95845)}$ erythrocytes as a likely mechanism for**
497 **increased clearance.**

498 Nevertheless, we hypothesized that this increase in RBC clearance is likely due to changes to
499 the cytoskeletal structure of *Ank-1*$^{(MRI95845/MRI95845)}$ RBCs. In order to examine our hypothesis,
500 we investigated the band 3 mobility within the RBC membrane as an indicator of the

501 integrity of vertical linkages in the RBC cytoskeleton [49,50]. We fluorescently labelled
502 erythrocytic band 3 with eosin-5'-maleimide and performed Fluorescence Recovery after
503 Photobleaching (FRAP) on erythrocytes, which involves photobleaching a spot on the RBC
504 surface with a pulse from a high-powered laser followed by a fluorescence recovery period
505 where the intensity was recorded over 5 minutes as a marker of mobility. *Ank-*
506 *1*$^{(MRI95845/MRI95845)}$ RBCs were found to have significantly higher fluorescence recovery
507 compared to wild-type and *Ank-1*$^{(MRI96570/+)}$ RBCs (Figure 4F), which suggests a higher band 3
508 mobility in *Ank-1*$^{(MRI95845/MRI95845)}$ erythrocytes, possibly due to an increased amount of band
509 3 that was not associated with the RBC cytoskeleton as the result of disrupted ankyrin
510 binding to band 3 on RBC surface.

511

512 **Discussion**

513 ***Ank-1* gene displayed allele-dependent heterogeneous phenotypes during malaria**
514 **infections**

515 Similar to HS in human populations, ankyrin mutations in mice also exhibit differences in
516 clinical symptoms depending on the mutations. As shown in this study, homozygosity for
517 MRI96570 mutation is lethal, while MRI95845 homozygotes appeared healthy; whereas
518 both *Ank-1*$^{(MRI96570/+)}$ mice and *Ank-1*$^{(MRI95845/+)}$ mice exhibited HS-phenotypes with similar
519 severity. While both mutations also conferred malaria protection and appeared to impair
520 parasite invasion, they also showed some remarkable differences in mediating this
521 resistance. Parasites in *Ank-1*$^{(MRI96570/+)}$ erythrocytes were more likely to be TUNEL-positive,
522 indicating impaired intra-erythrocytic maturation, whereas *Ank-1*$^{(MRI95845/MRI95845)}$

523 erythrocytes were more likely to be removed from circulation and possibly had an increased
524 turnover rate.

525 These findings were not exclusive to the two *Ank-1* mice described in this study. In fact,
526 previous studies on other *Ank-1* mice also exhibit similar mechanisms of resistance. Notably,
527 similar to $1^{(MRI96570/+)}$, $Ank\text{-}1^{(MRI23420/+)}$ [36] and $Ank\text{-}1^{(nb/nb)}$ mice [33] were both reported to
528 affect the parasite survival within the defective RBCs. These mutations resulted in truncated
529 protein, therefore, it is possible that the loss of C-terminal ANK-1 protein might be
530 important for growth. However, $Ank\text{-}1^{(MRI61689/+)}$ mice, which were also predicted to give rise
531 to truncated protein, were found to exhibit increased RBC bystander clearance but no intra-
532 erythrocytic growth impairment [41], similar to the $Ank\text{-}1^{(MRI95845/MRI95845)}$ mice in this study.

533 Taking these findings together, it would seem that although these mutations resides in
534 different exons of ankyrin-1 gene, they all resulted in HS-like phenotype. However, they
535 exert different effects on the parasite survival depending on the nature of the mutation. In
536 particular, nonsense mutations ($Ank\text{-}1^{(nb)}$, $Ank\text{-}1^{(MRI23420)}$, $Ank\text{-}1^{(MRI96570)}$), with the exception
537 of $Ank\text{-}1^{(MRI61689)}$, impair parasite growth. On the other hand, the only described missense
538 mutation, $Ank\text{-}1^{(MRI95845)}$, increases the bystander RBC clearance. It is interesting to note that
539 although $Ank\text{-}1^{(MRI61689)}$ mutation was predicted to produce a truncated protein, a full length
540 alternative spliced transcript with a skipped exon was also found [41], possibly indicating
541 that $Ank\text{-}1^{(MRI61689)}$ is unlikely to be a null mutation, consequently exhibiting different
542 mechanisms of malaria resistance compared to other nonsense mutations. Therefore, it is
543 proposed that the presence of a truncated form of ANK-1 protein might be important factor
544 to determine the detrimental effects on malaria parasites.

545 However, without detailed examination into RBC cytoskeletal structure, it is challenging to
546 speculate the exact mechanisms of malaria resistance of these mutations. Nevertheless, this
547 is the first direct report of such allelic heterogeneity described in *in vivo* malaria mouse
548 models, highlighting the complexity underlying the genetic resistance to malaria, which is
549 likely to correlate with human populations.

550

551 **Allelic heterogeneity of *Ank-1* and its association with malaria**

552 Due to lack of large scale studies on the HS prevalence in malaria endemic regions, ankyrin-1
553 mutations have not been associated with malaria protection. Although HS prevalence is
554 more well-characterized in non-malarial regions such as Northern European and Japanese
555 populations, with a prevalence of about 1 in 2000 [51-53], one study proposed an increased
556 HS incidence in Algeria of about 1 in 1000 [54], raising the possibility of positive selection of
557 HS by malarial parasites. However, as the result of extreme allelic heterogeneity of HS-
558 causing genes, many alleles do not reach sufficient frequencies [55] or achieve consistent
559 symptoms [56] to be easily associated with malaria protection. In addition, technical
560 difficulties [29], confounding factors from large genetic variation in African populations [57],
561 as well as poor diagnostics and health systems [57], pose significant challenges for
562 dissecting the connection between HS and malaria. Furthermore, the varying allele
563 frequency in African populations might introduce epistasis effects, possibly masking the
564 genotype-phenotype associated typically observed in other populations [58]. With
565 development of more advanced technologies and better characterization of the genetic
566 structure of African populations, further studies into the association of HS and malaria could

567 potentially yield beneficial insights into the co-evolutionary relationships between humans
568 and *Plasmodium*.

569 Nonetheless, previous *in vivo* studies have indicated that *Ank-1* mutations affect merozoite
570 invasion and maturation [33,36], both of which were also demonstrated in this study.
571 However, this study also describes for the first time, the direct *in vivo* observation of
572 different mutations in the *Ank-1* gene mediating two distinct, independent mechanisms of
573 malaria resistance, where one impairs parasite maturation and the other increases RBC
574 clearance. Ankyrin is one of the key proteins involved in RBC remodeling by parasites [59-
575 61], and maintaining the native structure of the RBC cytoskeleton [28,62]. It is possible that
576 this allelic heterogeneity is due to the effect each mutation has on the integrity of the RBC
577 cytoskeletal structure, as evidenced by the significantly increased band 3 mobility caused by
578 *Ank-1*$^{(MRI95845)}$, but not *Ank-1*$^{(MRI96570)}$ mutation (Figure 4F). This suggests that mutations at
579 different locations of the ankyrin-1 protein might have different effects on the RBCs,
580 consequently impacting the ability of parasites to invade and grow, which could be the basis
581 for further studies, while also taking into potential confounding factors due to differences in
582 genetic background.

583

584 **Similarities of allelic heterogeneity in *Ank-1* and other malaria susceptibility genes**

585 As evidenced from this study, the protective effect of the *Ank-1* gene against malaria is
586 dependent on the nature and the location of mutations within the gene. Similarly, this allelic
587 heterogeneity is also observed in other malaria susceptibility genes in human populations.
588 For instance, although many G6PD deficiency-causing alleles have been implicated with
589 malaria protection [63,64], the protective effects are often debated, with many studies

590 reporting increased, or no protection, for individuals with certain alleles of G6PD deficiency
591 [65-70]. This is thought to be due to the phenotypic complexity of G6PD deficiency
592 associated with malaria susceptibility [7]. Indeed, various G6PD alleles have been shown to
593 cause a reduction of G6PD activity with differing severity, and were proposed to correlate
594 with the malaria protection they conferred [65]. More recently, Clarke and colleagues
595 proposed reduced G6PD activity is associated with lower risk of cerebral malaria, but in
596 exchange for higher risk of malarial anemia [12], suggesting a delicate balance underlying
597 the high frequency of G6PD polymorphism of populations in malaria endemic region.
598 Similarly, *Ank-1* mutations described in this study, as well as other previous mouse studies
599 [33,35,36], exhibit variability in malaria resistance, most likely as the result of allelic
600 heterogeneity.

601 The heterogeneity in malaria resistance mechanisms of the *Ank-1* gene as observed in this
602 study is comparable to the two prevalent alleles of the β-globin gene – the HbS and HbC,
603 which result from amino acid substitution at position 6 from glutamate to either valine, or
604 lysine, respectively. These two mutations exhibit some similarities in mediating malaria
605 resistance, including impaired parasite growth [71,72], reduced cytoadherence [73-75] and
606 increased erythrocyte clearance [76]. However, HbS erythrocytes were found to be more
607 resistant to all forms of malaria, whereas HbC erythrocytes appeared to be protective
608 against cerebral malaria [15]. This difference in malaria protection was proposed to
609 correlate with distribution of HbS and HbC in Africa [16], further emphasizing the
610 importance of allelic heterogeneity in understanding host-parasite interactions.

611 In conclusion, we have reported a novel observation where the *Ank-1* gene exhibits
612 phenotypic heterogeneity in malaria resistance mechanisms, either by impairing intra-

613 erythrocytic parasite growth, or promoting RBC clearance. This study also highlighted that
614 the allelic heterogeneity in relation to malaria resistance is not exclusive to G6PD deficiency,
615 and it could also be much more common than we expected. Further studies should extend
616 the understanding of the effects of various *Ank-1* mutations on the development of intra-
617 erythrocytic parasites, as well as the association of HS with malaria in human populations.
618 This could provide new insights into the intricate relationships between RBC cytoskeletal
619 structure and parasite interactions.

620

621

622 **Acknowledgement**

623 We would like to acknowledge Shelley Lampkin and Australian Phenomics Facility (APF) for
624 the maintenance of the mouse colonies. We would also like to thank Dr Matthew Dixon and
625 Prof Leann Tilley for assisting with ektacytometry and FRAP techniques and the associated
626 analyses. We are also grateful for the assistance of the Microscopy Unit of the Macquarie
627 University in the sample preparation and operation of the scanning electron microscope.

628

629 1. Kwiatkowski DP (2005) How malaria has affected the human genome and what human
630 genetics can teach us about malaria. Am J Hum Genet 77: 171-192.
631 2. Hedrick PW (2012) Resistance to malaria in humans: the impact of strong, recent
632 selection. Malaria Journal 11: 349.
633 3. Williams TN (2006) Red blood cell defects and malaria. Mol Biochem Parasitol 149: 121-
634 127.
635 4. Williams TN (2006) Human red blood cell polymorphisms and malaria. Curr Opin
636 Microbiol 9: 388-394.
637 5. Lell B, May J, Schmidt-Ott RJ, Lehman LG, Luckner D, et al. (1999) The role of red blood
638 cell polymorphisms in resistance and susceptibility to malaria. Clin Infect Dis 28: 794-
639 799.

640 6. Fry AE, Ghansa A, Small KS, Palma A, Auburn S, et al. (2009) Positive selection of a CD36
641 nonsense variant in sub-Saharan Africa, but no association with severe malaria
642 phenotypes. Hum Mol Genet 18: 2683-2692.
643 7. Clark T, Fry A, Auburn S, Campino S, Diakite M, et al. (2009) Allelic heterogeneity of G6PD
644 deficiency in West Africa and severe malaria susceptibility. Eur J Hum Genet 17.
645 8. Bauduer F (2013) Red cell polymorphisms and malaria: an evolutionary approach.
646 Bulletins et mémoires de la Société d'anthropologie de Paris 25: 55-64.
647 9. Beutler E, Kuhl W, Sáenz GF, Rodríguez W (1991) Mutation analysis of glucose-6-
648 phosphate dehydrogenase (G6PD) variants in Costa Rica. Hum Genet 87.
649 10. Howes RE, Battle KE, Satyagraha AW, Baird JK, Hay SI (2013) G6PD deficiency: Global
650 distribution, genetic variants and primaquine therapy. Adv Parasitol 81.
651 11. Shah SS, Rockett KA, Jallow M, Sisay-Joof F, Bojang KA, et al. (2016) Heterogeneous
652 alleles comprising G6PD deficiency trait in West Africa exert contrasting effects on
653 two major clinical presentations of severe malaria. Malaria Journal 15: 1-8.
654 12. Clarke GM, Rockett K, Kivinen K, Hubbart C, Jeffreys AE, et al. (2017) Characterisation of
655 the opposing effects of G6PD deficiency on cerebral malaria and severe malarial
656 anaemia. eLife 6: e15085.
657 13. Kilian N, Srismith S, Dittmer M, Ouermi D, Bisseye C, et al. (2015) Hemoglobin S and C
658 affect protein export in *Plasmodium falciparum*-infected erythrocytes. Biology Open
659 4: 400-410.
660 14. May J, Evans JA, Timmann C, Ehmen C, Busch W, et al. (2007) Hemoglobin variants and
661 disease manifestations in severe *falciparum* malaria. JAMA 297: 2220-2226.
662 15. Kreuels B, Kreuzberg C, Kobbe R, Ayim-Akonor M, Apiah-Thompson P, et al. (2010)
663 Differing effects of HbS and HbC traits on uncomplicated *falciparum* malaria, anemia,
664 and child growth. Blood 115: 4551-4558.
665 16. Gonçalves BP, Gupta S, Penman BS (2016) Sickle haemoglobin, haemoglobin C and
666 malaria mortality feedbacks. Malaria Journal 15: 26.
667 17. Aitman TJ, Cooper LD, Norsworthy PJ, Wahid FN, Gray JK, et al. (2000) Malaria
668 susceptibility and CD36 mutation. Nature 405: 1015-1016.
669 18. Curtis BR, Aster RH (1996) Incidence of the Nak(a)-negative platelet phenotype in African
670 Americans is similar to that of Asians. Transfusion 36: 331-334.
671 19. Urwijitaroon Y, Barusrux S, Romphruk A, Puapairoj C (1995) Frequency of human platelet
672 antigens among blood donors in northeastern Thailand. Transfusion 35: 868-870.
673 20. Pain A, Urban BC, Kai O, Casals-Pascual C, Shafi J, et al. (2001) A non-sense mutation in
674 Cd36 gene is associated with protection from severe malaria. Lancet 357: 1502-1503.
675 21. Amodu OK, Gbadegesin RA, Ralph SA, Adeyemo AA, Brenchley PE, et al. (2005)
676 *Plasmodium falciparum* malaria in south-west Nigerian children: is the
677 polymorphism of ICAM-1 and E-selectin genes contributing to the clinical severity of
678 malaria? Acta Trop 95: 248-255.
679 22. Ayodo G, Price AL, Keinan A, Ajwang A, Otieno MF, et al. (2007) Combining evidence of
680 natural selection with association analysis increases power to detect malaria-
681 resistance variants. Am J Hum Genet 81: 234-242.
682 23. Gallagher PG, Forget BG (1998) Hematologically Important Mutations: Spectrin and
683 Ankyrin Variants in Hereditary Spherocytosis. Blood Cells, Molecules, and Diseases
684 24: 539-543.

685 24. Jarolim P, Murray JL, Rubin HL, Taylor WM, Prchal JT, et al. (1996) Characterization of 13
686 novel band 3 gene defects in hereditary spherocytosis with band 3 deficiency. Blood
687 88: 4366-4374.
688 25. Takaoka Y, Ideguchi H, Matsuda M, Sakamoto N, Takeuchi T, et al. (1994) A novel
689 mutation in the erythrocyte protein 4.2 gene of Japanese patients with hereditary
690 spherocytosis (protein 4.2 Fukuoka). Br J Haematol 88: 527-533.
691 26. Matsuda M, Hatano N, Ideguchi H, Takahira H, Fukumaki Y (1995) A novel mutation
692 causing an aberrant splicing in the protein 4.2 gene associated with hereditary
693 spherocytosis (protein 4.2Notame). Hum Mol Genet 4: 1187-1191.
694 27. Eber SW, Gonzalez JM, Lux ML, Scarpa AL, Tse WT, et al. (1996) Ankyrin-1 mutations are
695 a major cause of dominant and recessive hereditary spherocytosis. Nat Genet 13:
696 214-218.
697 28. Gallagher PG (2005) Hematologically important mutations: ankyrin variants in hereditary
698 spherocytosis. Blood Cells Mol Dis 35: 345-347.
699 29. Sangerman J, Maksimova Y, Edelman EJ, Morrow JS, Forget BG, et al. (2008) Ankyrin-
700 linked hereditary spherocytosis in an African-American kindred. Am J Hematol 83:
701 789-794.
702 30. Spector I, Metz J (1963) A Bantu family with hereditary spherocytosis. S Afr Med J 37:
703 211-213.
704 31. Hassan A, Babadoko AA, Isa AH, Abunimye P (2009) Hereditary spherocytosis in a 27-
705 year-old woman: case report. Ann Afr Med 8: 61-63.
706 32. Ustun C, Kutlar F, Holley L, Seigler M, Burgess R, et al. (2003) Interaction of sickle cell
707 trait with hereditary spherocytosis: splenic infarcts and sequestration. Acta
708 Haematol 109: 46-49.
709 33. Shear HL, Roth EF, Jr., Ng C, Nagel RL (1991) Resistance to malaria in ankyrin and
710 spectrin deficient mice. Br J Haematol 78: 555-560.
711 34. Schulman S, Roth EF, Jr., Cheng B, Rybicki AC, Sussman, II, et al. (1990) Growth of
712 *Plasmodium falciparum* in human erythrocytes containing abnormal membrane
713 proteins. Proc Natl Acad Sci U S A 87: 7339-7343.
714 35. Rank G, Sutton R, Marshall V, Lundie RJ, Caddy J, et al. (2009) Novel roles for erythroid
715 Ankyrin-1 revealed through an ENU-induced null mouse mutant. Blood 113: 3352-
716 3362.
717 36. Greth A, Lampkin S, Mayura-Guru P, Rodda F, Drysdale K, et al. (2012) A novel ENU-
718 mutation in ankyrin-1 disrupts malaria parasite maturation in red blood cells of mice.
719 PLoS One 7: e38999.
720 37. Hortle E, Nijagal B, Bauer DC, Jensen LM, Ahn SB, et al. (2016) Adenosine
721 monophosphate deaminase 3 activation shortens erythrocyte half-life and provides
722 malaria resistance in mice. Blood.
723 38. Bauer DC, McMorran BJ, Foote SJ, Burgio G (2015) Genome-wide analysis of chemically
724 induced mutations in mouse in phenotype-driven screens. BMC Genomics 16: 1-8.
725 39. Wang K, Li M, Hakonarson H (2010) ANNOVAR: functional annotation of genetic variants
726 from high-throughput sequencing data. Nucleic Acids Research 38: e164-e164.
727 40. Deplaine G, Safeukui I, Jeddi F, Lacoste F, Brousse V, et al. (2011) The sensing of poorly
728 deformable red blood cells by the human spleen can be mimicked in vitro. Blood 117:
729 e88-95.

730 41. Huang HM, Bauer DC, Lelliott PM, Greth A, McMorran BJ, et al. (2016) A novel ENU-
731 induced ankyrin-1 mutation impairs parasite invasion and increases erythrocyte
732 clearance during malaria infection in mice. Sci Rep 6: 37197.
733 42. Livak KJ, Schmittgen TD (2001) Analysis of relative gene expression data using real-time
734 quantitative PCR and the 2− ΔΔCT method. methods 25: 402-408.
735 43. Schneider CA, Rasband WS, Eliceiri KW (2012) NIH Image to ImageJ: 25 years of image
736 analysis. Nat Meth 9: 671-675.
737 44. Jarra W, Brown K (1985) Protective immunity to malaria: studies with cloned lines of
738 *Plasmodium chabaudi* and *P. berghei* in CBA/Ca mice. I. The effectiveness and inter-
739 and intra-species specificity of immunity induced by infection. Parasite immunology
740 7: 595-606.
741 45. Lelliott PM, Lampkin S, McMorran BJ, Foote SJ, Burgio G (2014) A flow cytometric assay
742 to quantify invasion of red blood cells by rodent *Plasmodium* parasites in vivo. Malar
743 J 13: 100.
744 46. Lelliott PM, McMorran BJ, Foote SJ, Burgio G (2015) *In vivo* assessment of rodent
745 *Plasmodium parasitemia* and merozoite invasion by flow cytometry. JoVE (Journal of
746 Visualized Experiments): e52736-e52736.
747 47. Chishti AH, Palek J, Fisher D, Maalouf GJ, Liu SC (1996) Reduced invasion and growth of
748 *Plasmodium falciparum* into elliptocytic red blood cells with a combined deficiency
749 of protein 4.1, glycophorin C, and p55. Blood 87: 3462-3469.
750 48. McMorran BJ, Marshall VM, de Graaf C, Drysdale KE, Shabbar M, et al. (2009) Platelets
751 Kill Intraerythrocytic Malarial Parasites and Mediate Survival to Infection. Science
752 323: 797-800.
753 49. Kodippili GC, Spector J, Sullivan C, Kuypers FA, Labotka R, et al. (2009) Imaging of the
754 diffusion of single band 3 molecules on normal and mutant erythrocytes. Blood 113:
755 6237-6245.
756 50. Cho MR, Eber SW, Liu S-C, Lux SE, Golan DE (1998) Regulation of Band 3 Rotational
757 Mobility by Ankyrin in Intact Human Red Cells. Biochemistry 37: 17828-17835.
758 51. Godal HC, Heisto H (1981) High prevalence of increased osmotic fragility of red blood
759 cells among Norwegian blood donors. Scand J Haematol 27: 30-34.
760 52. Eber SW, Pekrun A, Neufeldt A, Schroter W (1992) Prevalence of increased osmotic
761 fragility of erythrocytes in German blood donors: screening using a modified glycerol
762 lysis test. Ann Hematol 64: 88-92.
763 53. Yawata Y, Kanzaki A, Yawata A, Doerfler W, Ozcan R, et al. (2000) Characteristic features
764 of the genotype and phenotype of hereditary spherocytosis in the Japanese
765 population. Int J Hematol 71: 118-135.
766 54. Zerhouni F, Guetarni D, Henni T, Colonna P (1991) Occurrence and characteristics of
767 hereditary spherocytosis in Algeria. Eur J Haematol 47: 42-47.
768 55. Kavallaris M, Ng D, Byrne F (2012) Cytoskeleton and Human Disease: Springer.
769 56. Shah S, Vega R (2004) Hereditary Spherocytosis. Pediatrics in Review 25: 168-172.
770 57. (2008) A global network for investigating the genomic epidemiology of malaria. Nature
771 456: 732-737.
772 58. Greene CS, Penrod NM, Williams SM, Moore JH (2009) Failure to replicate a genetic
773 association may provide important clues about genetic architecture. PLoS One 4:
774 e5639.

775 59. Maier AG, Cooke BM, Cowman AF, Tilley L (2009) Malaria parasite proteins that remodel
776 the host erythrocyte. Nat Rev Micro 7: 341-354.
777 60. Zuccala ES, Baum J (2011) Cytoskeletal and membrane remodelling during malaria
778 parasite invasion of the human erythrocyte. Br J Haematol 154: 680-689.
779 61. Hanspal M, Dua M, Takakuwa Y, Chishti AH, Mizuno A (2002) *Plasmodium falciparum*
780 cysteine protease falcipain-2 cleaves erythrocyte membrane skeletal proteins at late
781 stages of parasite development. Presented in part in abstract form at the 43rd
782 Annual Meeting of the American Society of Hematology, Orlando, FL, 2001 100:
783 1048-1054.
784 62. Miraglia del Giudice E, Iolascon A, Pinto L, Nobili B, Perrotta S (1994) Erythrocyte
785 membrane protein alterations underlying clinical heterogeneity in hereditary
786 spherocytosis. Br J Haematol 88: 52-55.
787 63. Ruwende C, Hill A (1998) Glucose-6-phosphate dehydrogenase deficiency and malaria. J
788 Mol Med (Berl) 76: 581-588.
789 64. Mason PJ, Bautista JM, Gilsanz F (2007) G6PD deficiency: the genotype-phenotype
790 association. Blood Rev 21.
791 65. Manjurano A, Sepulveda N, Nadjm B, Mtove G, Wangai H, et al. (2015) African glucose-6-
792 phosphate dehydrogenase alleles associated with protection from severe malaria in
793 heterozygous females in Tanzania. PLoS Genet 11.
794 66. Ruwende C, Khoo SC, Snow RW, Yates SN, Kwiatkowski D, et al. (1995) Natural selection
795 of hemi- and heterozygotes for G6PD deficiency in Africa by resistance to severe
796 malaria. Nature 376.
797 67. Guindo A, Fairhurst RM, Doumbo OK, Wellems TE, Diallo DA (2007) X-Linked G6PD
798 Deficiency Protects Hemizygous Males but Not Heterozygous Females against Severe
799 Malaria. PLoS Medicine 4: e66.
800 68. Sirugo G, Predazzi IM, Bartlett J, Tacconelli A, Walther M, et al. (2014) G6PD A-
801 deficiency and severe malaria in The Gambia: heterozygote advantage and possible
802 homozygote disadvantage. Am J Trop Med Hyg 90.
803 69. Toure O, Konate S, Sissoko S, Niangaly A, Barry A, et al. (2012) Candidate polymorphisms
804 and severe malaria in a Malian population. PLoS One 7: e43987.
805 70. Martin SK, Miller LH, Alling D, Okoye VC, Esan GJ, et al. (1979) Severe malaria and
806 glucose-6-phosphate-dehydrogenase deficiency: a reappraisal of the malaria/G-6-P.D.
807 hypothesis. Lancet 1.
808 71. Fairhurst RM, Fujioka H, Hayton K, Collins KF, Wellems TE (2003) Aberrant development
809 of *Plasmodium falciparum* in hemoglobin CC red cells: implications for the malaria
810 protective effect of the homozygous state. Blood 101: 3309-3315.
811 72. Cyrklaff M, Sanchez CP, Kilian N, Bisseye C, Simpore J, et al. (2011) Hemoglobins S and C
812 interfere with actin remodeling in *Plasmodium falciparum*-infected erythrocytes.
813 Science 334: 1283-1286.
814 73. Carlson J, Nash GB, Gabutti V, al Yaman F, Wahlgren M (1994) Natural protection against
815 severe *Plasmodium falciparum* malaria due to impaired rosette formation. Blood 84.
816 74. Fairhurst RM, Bess CD, Krause MA (2012) Abnormal PfEMP1/knob display on
817 *Plasmodium falciparum*-infected erythrocytes containing hemoglobin variants: fresh
818 insights into malaria pathogenesis and protection. Microbes and Infection / Institut
819 Pasteur 14: 851-862.

820 75. Fairhurst RM, Baruch DI, Brittain NJ, Ostera GR, Wallach JS, et al. (2005) Abnormal
821 display of PfEMP-1 on erythrocytes carrying haemoglobin C may protect against
822 malaria. Nature 435: 1117-1121.
823 76. Ayi K, Turrini F, Piga A, Arese P (2004) Enhanced phagocytosis of ring-parasitized mutant
824 erythrocytes: a common mechanism that may explain protection against *falciparum*
825 malaria in sickle trait and beta-thalassemia trait. Blood 104: 3364-3371.

826

827

828 **Figure Captions**

829 **Figure 1. The mutations and phenotypes of *Ank-1*$^{(MRI96570/+)}$, *Ank-1*$^{(MRI95845/+)}$ and *Ank-*
830 ***1***$^{(MRI95845/MRI95845)}$ **mice.** (A) The location of ankyrin-1 mutations in *Ank-1*$^{(MRI96570)}$ and *Ank-*
831 *1*$^{(MRI95845)}$ alleles and the predicted effects on ankyrin-1 protein, compared to the previously
832 described *Ank-1*$^{(MRI23420)}$, *Ank-1*$^{(MRI61689)}$ and *Ank-1*$^{(nb)}$. (B) The *Ank-1*$^{(MRI96570/MRI96570)}$ pups
833 (indicated by arrows) showed severe jaundice and died within 1 week after birth. (C) The
834 osmotic fragility of *Ank-1*$^{(MRI96570/+)}$, *Ank-1*$^{(MRI95845/+)}$ and *Ank-1*$^{(MRI95845/MRI95845)}$ erythrocytes in
835 hypotonic solution from 0-10g/L sodium (n=5). (D) The RBC half-life of *Ank-1*$^{(MRI96570/+)}$, *Ank-*
836 *1*$^{(MRI95845/+)}$ and *Ank-1*$^{(MRI95845/MRI95845)}$ mice (n=5). (E) The elasticity of *Ank-1*$^{(MRI96570/+)}$ and
837 *Ank-1*$^{(MRI95845/MRI95845)}$ RBCs under shear pressure as measured by ektacytometer (n=3). (F)
838 The proportion of retained *Ank-1*$^{(MRI96570/+)}$, *Ank-1*$^{(MRI95845/+)}$ and *Ank-1*$^{(MRI95845/MRI95845)}$ RBCs
839 when passing through a layer of beads during the *in vitro* spleen retention assay (n=3). *
840 P<0.05, ** P<0.01, *** P<0.001. All error bars indicate standard error of mean (SEM).

841

842 **Figure 2. The parasitemia and survival of *Ank-1*$^{(MRI96570/+)}$, *Ank-1*$^{(MRI95845/+)}$ and *Ank-*
843 ***1***$^{(MRI95845/MRI95845)}$ **mice during *P. chabaudi* infection.** (A) The parasite load and (B) survival
844 rate of *Ank-1*$^{(MRI96570/+)}$, *Ank-1*$^{(MRI95845/+)}$ and *Ank-1*$^{(MRI95845/MRI95845)}$ mice from two

845 independent experiments, starting from day 7 to day 15 post-infection when challenged
846 with $1x10^4$ parasite intraperitoneally as determined by light microscopy. (n=9-13). * P<0.05,
847 *** P<0.001. Error bars indicate SEM.

848

849 **Figure 3. The parasite invasion and intra-erythrocytic growth as indicated via IVET and**
850 **TUNEL assay.** The relative invasion efficiency into *Ank-1*$^{(MRI96570/+)}$ and *Ank-1*$^{(MRI95845/MRI95845)}$
851 erythrocytes was examined through IVET assay, where parasitemia ratio was calculated
852 from parasite load of either (A) *Ank-1*$^{(MRI96570/+)}$ to wild-type, (B) *Ank-1*$^{(MRI95845/MRI95845)}$ to
853 wild-type, or (C) *Ank-1*$^{(MRI96570/+)}$ to *Ank-1*$^{(MRI95845/MRI95845)}$ erythrocytes (n=5-7 per group). (D)
854 The parasite growth inhibition was determined via TUNEL assay on infected RBCs (DAPI-
855 positive) as an indicator of apoptotic and necrotic parasites. (E) The proportion of TUNEL-
856 positive infected RBCs was counted for *Ank-1*$^{(MRI96570/+)}$, *Ank-1*$^{(MRI95845/+)}$ and *Ank-*
857 *1*$^{(MRI95845/MRI95845)}$ mice at 1-5% parasitemia at ring stage (6-8 hours) and late trophozoite (18-
858 20 hours) stage (n=4). *P<0.05, **P<0.01, ***P<0.001. Error bars indicates SEM.

859

860 **Figure 4. The band 3 mobility and clearance of wild-type, *Ank-1*$^{(MRI96570/+)}$ and *Ank-***
861 ***1*$^{(MRI95845/MRI95845)}$ erythrocytes.** The remaining percentage of labelled RBCs was monitored
862 during the course of IVET assays, comparing between (A) wild-type and *Ank-1*$^{(MRI96570/+)}$
863 erythrocytes, (B) wild-type and *Ank-1*$^{(MRI95845/MRI95845)}$ erythrocytes, and (C) *Ank-1*$^{(MRI96570/+)}$
864 and *Ank-1*$^{(MRI95845/MRI95845)}$ erythrocytes (n=5-7). (D) The half-life of wild-type, *Ank-1*$^{(MRI96570/+)}$
865 *Ank-1*$^{(MRI95845/MRI95845)}$ erythrocytes during malaria infection as determined by biotinylation of
866 RBCs when parasites were detectable (n=6-7). (E) The clearance of wild-type and *Ank-*
867 *1*$^{(MRI95845/MRI95845)}$ erythrocytes in splenectomised and non-splenectomised mice infected

868 with *P. chabaudi* over 3 days starting from 1% parasitemia (n=6). (F) The band 3 mobility on
869 RBC membrane was measured using Fluorescence recovery after Photobleaching (FRAP),
870 showing the recovery rate of fluorescence as a result of Band 3 migration to the bleach spot
871 (n=9-21). ** P<0.01, *** P<0.001. Error bars indicate SEM.

872

873

874 **Supporting Information Captions**

875 **Table S1. The candidate genes for MRI96570 and MRI95845 mutations.** Variants from
876 exome sequencing were filtered to exclude strain-specific variants and variants found in
877 other ENU-induced mice. Variants that were shared between the two mice carrying
878 MRI96570 mutation or MRI95845 mutation are shown in (A) and (B), respectively. For each
879 mutation, the candidate genes were Sanger sequenced in affected mice to determine the
880 correlation between the genetic mutations and the phenotype by calculating the LOD score.
881 LOD Threshold = 1.9 for MRI96570, 2.0 for MRI95845 (n= 10).

882

883 **Figure S1. The location of *Ank-1*$^{(MRI96570)}$ and *Ank-1*$^{(MRI95845)}$ mutation.** (A) Sanger sequencing
884 of mice carrying *Ank-1*$^{(MRI96570)}$ revealed a T to A transversion in exon 34 of *Ank-1* gene,
885 which is predicted to induce a premature stop codon. (B) Mice carrying *Ank-1*$^{(MRI95845)}$
886 mutation were found to have a T to A transversion in exon 5 of *Ank-1* gene, which is
887 predicted to cause a missense mutation from tyrosine to asparagine at residue 149.

888

889 **Table S2. The complete blood count of *Ank-1*$^{(MRI96570/+)}$, *Ank-1*$^{(MRI95845/+)}$ and *Ank-*
890 ***1*$^{(MRI95845/MRI95845)}$ mice.** The blood parameters were obtained from a haematological
891 analyser ADVIA 120. WBC = white blood cell count; RBC = red blood cell count; HGB = total
892 haemoglobin; MCV = mean corpuscular volume; MCH = mean corpuscular haemoglobin;
893 MCHC = mean corpuscular haemoglobin concentration; RDW = red cell distribution width;
894 PLT = platelet counts; Retics = percentage of reticulocytes, n=23-50. Bonferroni adjusted
895 significance threshold = 0.001852, * P< 0.001, ** P< $1x10^{-5}$ compared to wild-type mice;
896 whereas ^ P<0.001 compared to *Ank-1*$^{(MRI95845/+)}$ mice.

897

898 **Figure S2. The RBC morphology of mice carrying *Ank-1*$^{(MRI96570)}$ or *Ank-1*$^{(MRI95845)}$ mutation.**
899 (A) Giemsa-stained blood smears as examined under light microscope at 1000x
900 magnification. (B) Scanning electron microscopic images showing the RBC shape of *Ank-*
901 *1*$^{(MRI96570/+)}$, *Ank-1*$^{(MRI95845/+)}$ and *Ank-1*$^{(MRI95845/MRI95845)}$ mice.

902

903 **Figure S3. The expression of *Ank-1* and other RBC cytoskeletal proteins in mice carrying**
904 ***Ank-1*$^{(MRI96570)}$ or *Ank-1*$^{(MRI95845)}$ mutation.** (A) Quantitative PCR was carried out on E14
905 embryonic livers to examine *Ank-1* expression levels (n=3). The abundance of ANK-1 and
906 other RBC cytoskeletal protein levels of *Ank-1*$^{(MRI96570/+)}$, *Ank-1*$^{(MRI95845/+)}$ and *Ank-*
907 *1*$^{(MRI95845/MRI95845)}$ mice as examined via (B) Coomassie staining and (C) Western blotting on
908 membrane of mature RBCs. (D) The relative abundance of various cytoskeletal protein levels
909 calculated from western blots (n=3). SPTA = α-spectrin, SPTB = β-spectrin, P 4.2 = Protein 4.2.
910 * P<0.05, ** P<0.01. Error bars indicate SEM.

911

912 **Figure S4. The parasitemia of the host mice during IVET assays and half-life assay.** The
913 parasitemia curve of the host mice during IVET assays, when comparing (A) wild-type with
914 *Ank-1*$^{(MRI95845/MRI95845)}$ erythrocytes, and (B) *Ank-1*$^{(MRI96570/+)}$ with *Ank-1*$^{(MRI95845/MRI95845)}$
915 erythrocytes (n=5-7). (C) The parasitemia curve of wild-type, *Ank-1*$^{(MRI96570/+)}$ and *Ank-*
916 *1*$^{(MRI95845/MRI95845)}$ mice during RBC half-life assay (n=6-7).

917

918

Figure 1

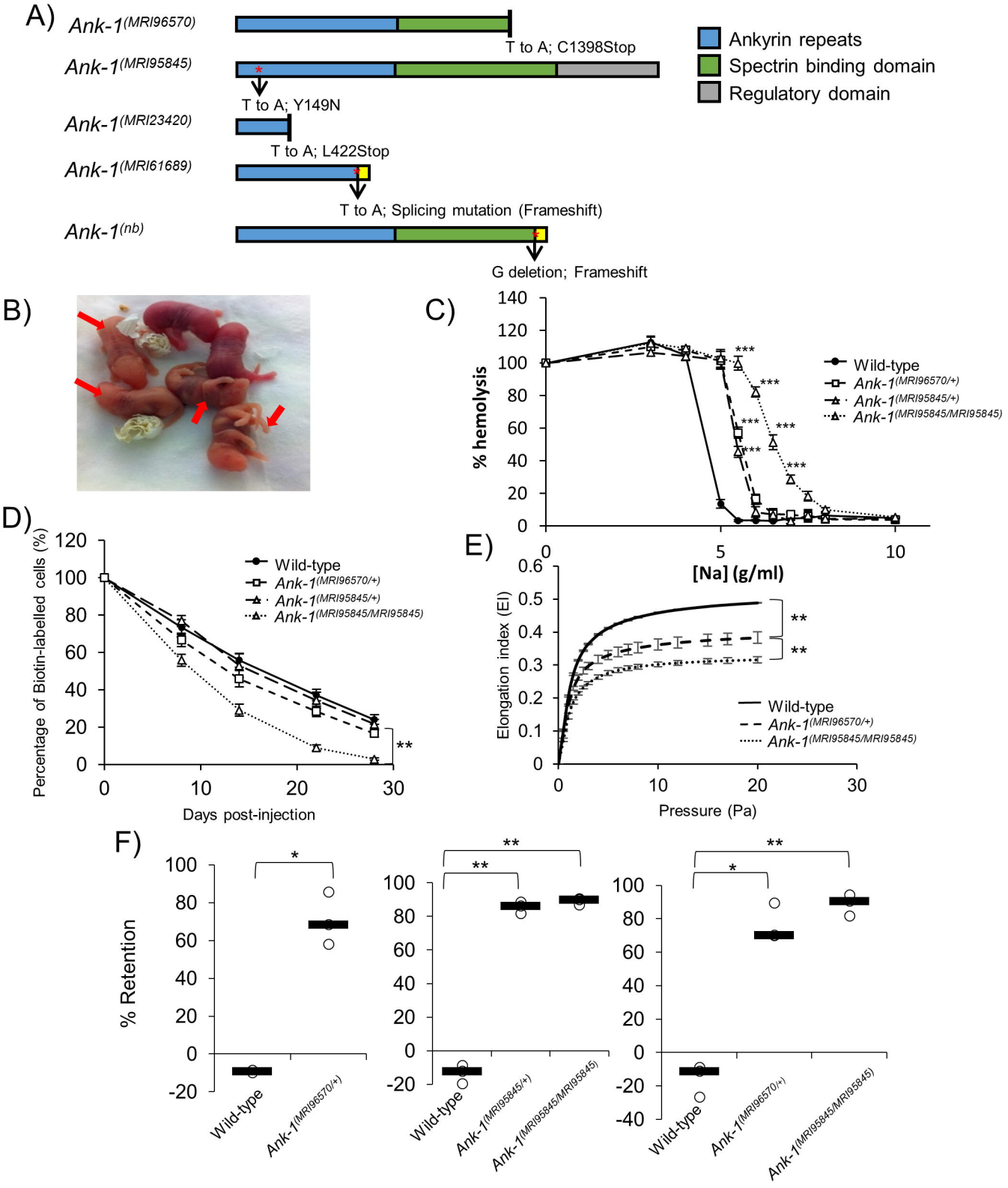
A)
Ank-1(MRI96570)
T to A; C1398Stop
Ank-1(MRI95845)
T to A; Y149N
Ank-1(MRI23420)
T to A; L422Stop
Ank-1(MRI61689)
T to A; Splicing mutation (Frameshift)
Ank-1(nb)
G deletion; Frameshift
Ankyrin repeats
Spectrin binding domain
Regulatory domain
B)
C)
% hemolysis
[Na] (g/ml)
Wild-type
Ank-1(MRI96570/+)
Ank-1(MRI95845/+)
Ank-1(MRI95845/MRI95845)
D)
Percentage of Biotin-labelled cells (%)
Days post-injection
E)
Elongation index (EI)
Pressure (Pa)
F)
% Retention

Figure 2

A)

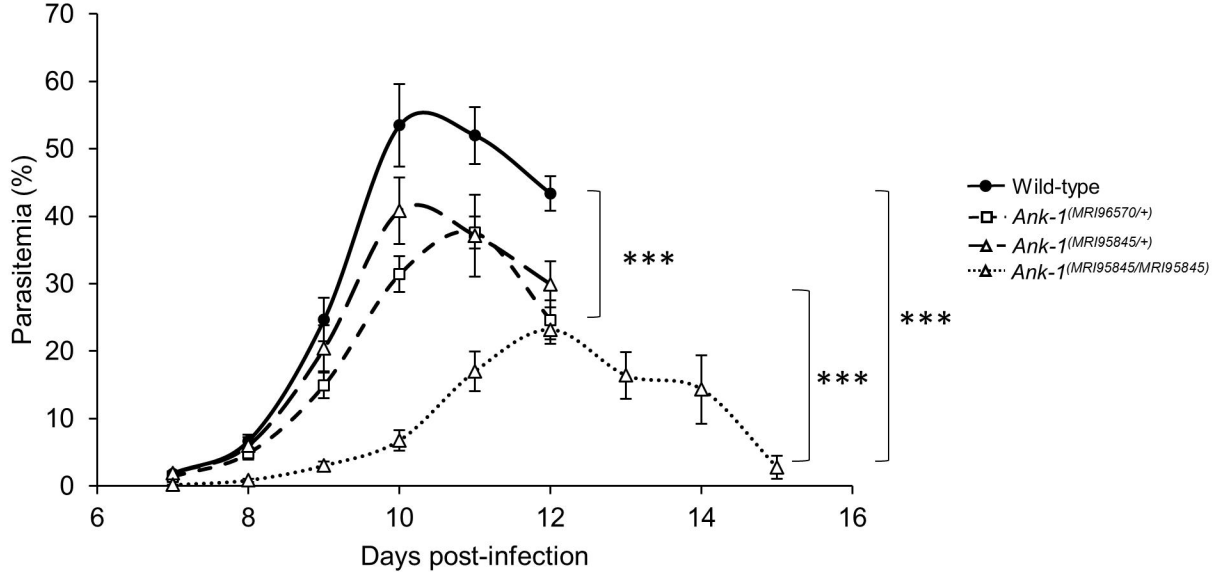
Parasitemia (%)
70
60
50
40
30
20
10
0
6
8
10
12
14
16
Days post-infection
***
***
***
Wild-type
Ank-1(MRI96570/+)
Ank-1(MRI95845/+)
Ank-1(MRI95845/MRI95845)

B)

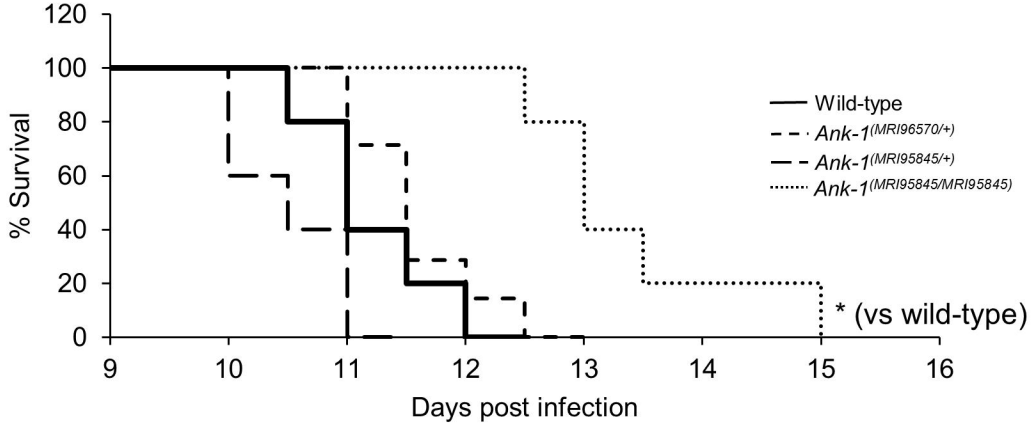
% Survival
120
100
80
60
40
20
0
9
10
11
12
13
14
15
16
Days post infection
Wild-type
Ank-1(MRI96570/+)
Ank-1(MRI95845/+)
Ank-1(MRI95845/MRI95845)
* (vs wild-type)

Figure 3

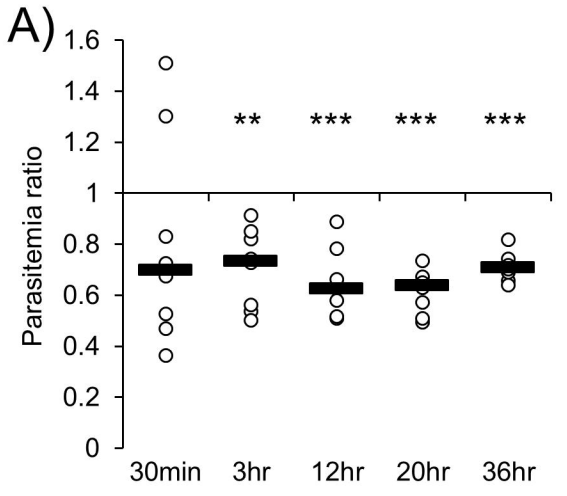
A)
Parasitemia ratio
1.6
1.4
1.2
1
0.8
0.6
0.4
0.2
0
**
***
***
***
30min
3hr
12hr
20hr
36hr

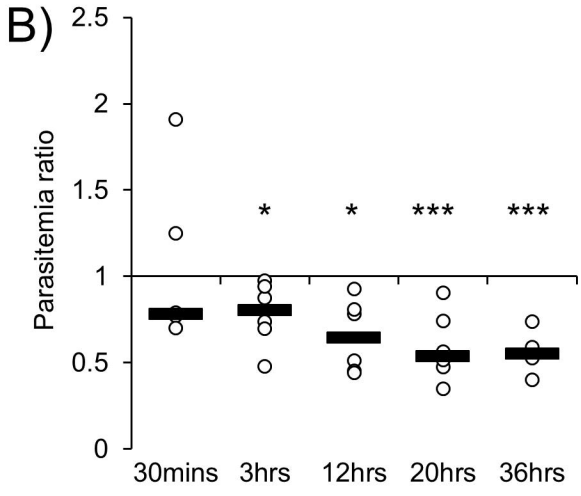
B)
Parasitemia ratio
2.5
2
1.5
1
0.5
0
*
*
***
***
30mins
3hrs
12hrs
20hrs
36hrs

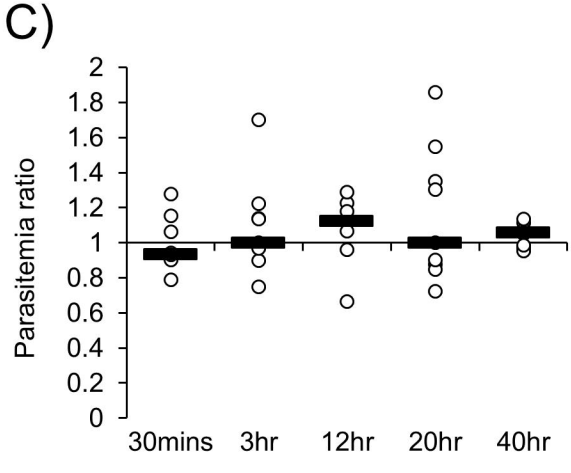
C)
Parasitemia ratio
2
1.8
1.6
1.4
1.2
1
0.8
0.6
0.4
0.2
0
30mins
3hr
12hr
20hr
40hr

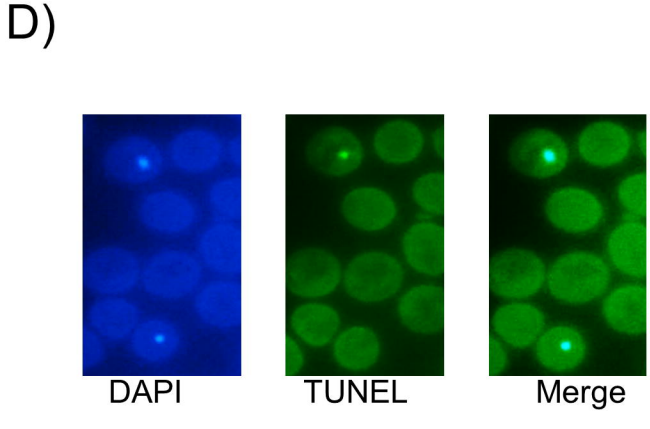
D)
DAPI
TUNEL
Merge

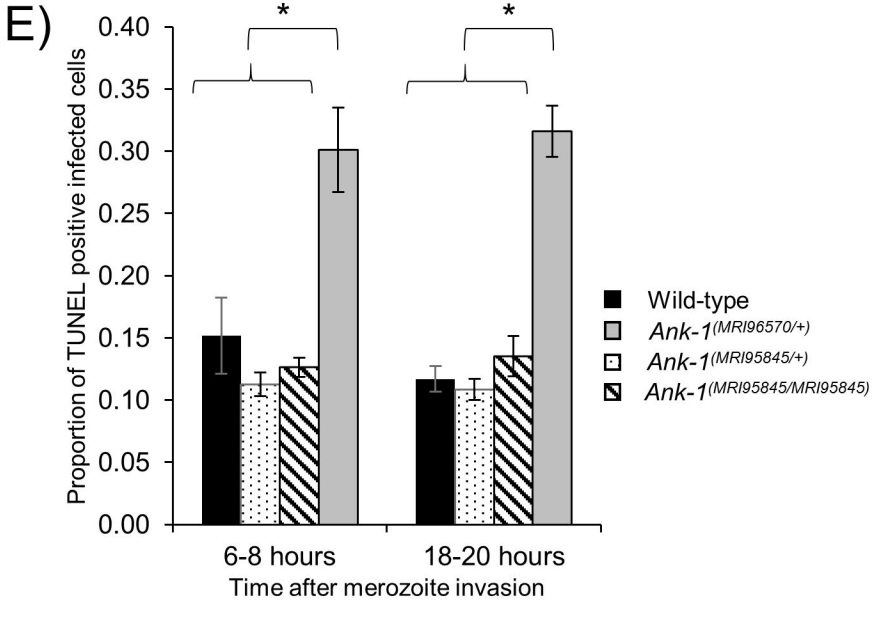
E)
Proportion of TUNEL positive infected cells
0.40
0.35
0.30
0.25
0.20
0.15
0.10
0.05
0.00
*
*
6-8 hours
18-20 hours
Time after merozoite invasion
Wild-type
Ank-1(MRI96570/+)
Ank-1(MRI95845/+)
Ank-1(MRI95845/MRI95845)

Figure 4

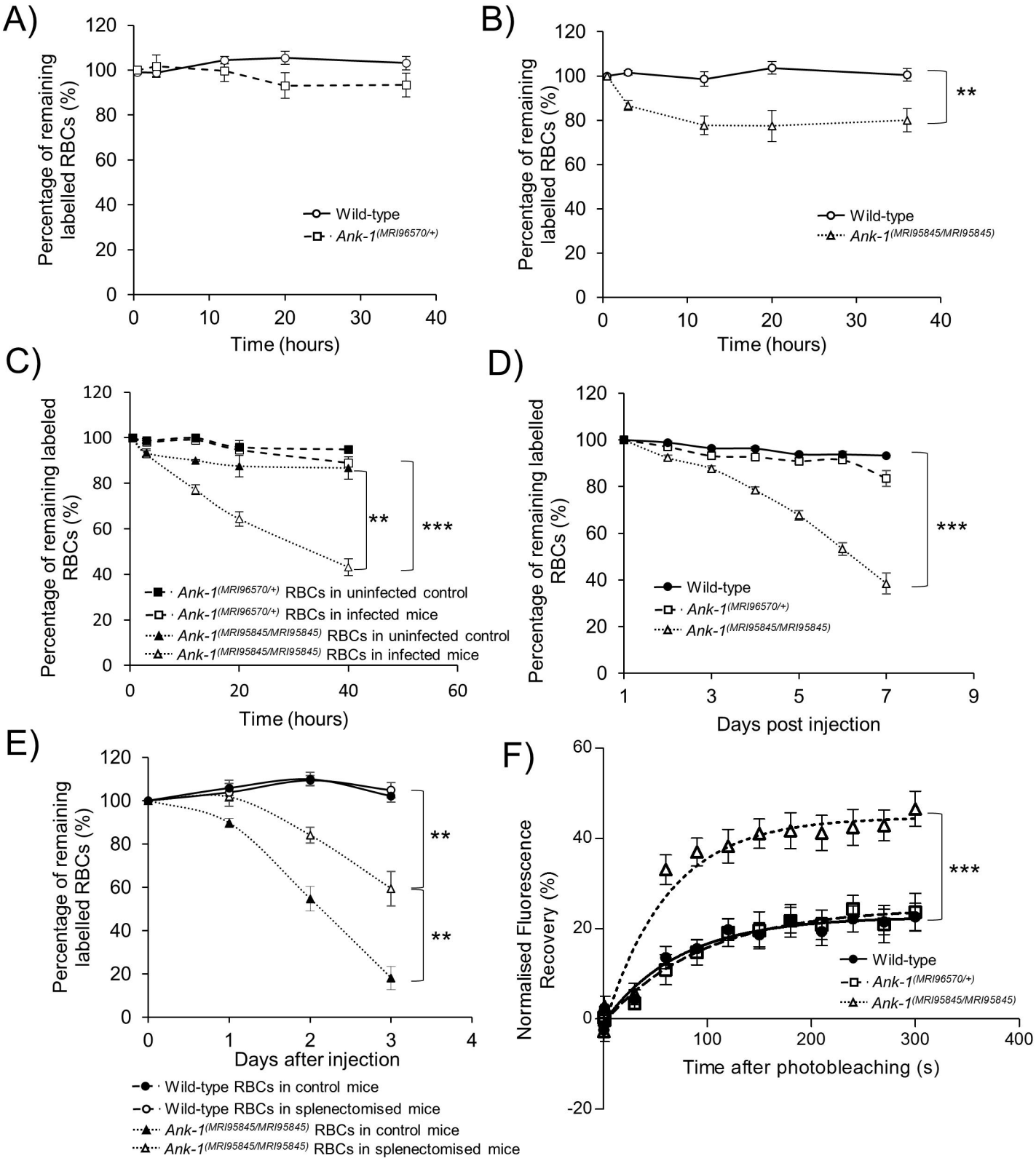
A)
Percentage of remaining labelled RBCs (%)
Time (hours)
Wild-type
Ank-1(MRI96570/+)
B)
Percentage of remaining labelled RBCs (%)
Time (hours)
**
Wild-type
Ank-1(MRI95845/MRI95845)
C)
Percentage of remaining labeled RBCs (%)
Time (hours)
**
***
Ank-1(MRI96570/+) RBCs in uninfected control
Ank-1(MRI96570/+) RBCs in infected mice
Ank-1(MRI95845/MRI95845) RBCs in uninfected control
Ank-1(MRI95845/MRI95845) RBCs in infected mice
D)
Percentage of remaining labelled RBCs (%)
Days post injection
***
Wild-type
Ank-1(MRI96570/+)
Ank-1(MRI95845/MRI95845)
E)
Percentage of remaining labelled RBCs (%)
Days after injection
**
**
Wild-type RBCs in control mice
Wild-type RBCs in splenectomised mice
Ank-1(MRI95845/MRI95845) RBCs in control mice
Ank-1(MRI95845/MRI95845) RBCs in splenectomised mice
F)
Normalised Fluorescence Recovery (%)
Time after photobleaching (s)
***
Wild-type
Ank-1(MRI96570/+)
Ank-1(MRI95845/MRI95845)

Table S1

Table S1. The candidate genes for MRI96570 and MRI95845 mutations.

A)

Chromosome	Gene name	Location	Reference base	Variant base	Number of mutant mice with mutation	LOD score (Threshold: 1.9)
3	*Fat4*	38888347	T	A	0/10	-2.81
7	*Rhcg*	79601661	T	C	0/10	-2.81
8	*Ank1*	23119400	T	A	10/10	2.81
X	*Plxnb3*	73763183	G	T	0/10	-2.81

B)

Chromosome	Gene name	Location	Reference base	Variant base	Number of mutant mice with mutation	LOD score (Threshold: 2.0)
8	*Ank1*	23085597	T	A	10/10	2.81
8	*Pnpla6*	3531116	G	A	8/10	1.24
9	*Zglp1*	21062907	G	A	0/10	-2.81
16	*Snai2*	14708259	A	C	0/10	-2.81
16	*Tbc1d23*	57191544	T	C	0/10	-2.81

Variants from exome sequencing were filtered to exclude strain-specific variants and variants found in other ENU-induced mice. Variants that were shared between the two mice carrying MRI96570 mutation or MRI95845 mutation are shown in (A) and (B), respectively. For each mutation, the candidate genes were Sanger sequenced in affected mice to determine the correlation between the genetic mutations and the phenotype by calculating the LOD score. LOD Threshold = 1.9 for MRI96570, 2.0 for MRI95845 (n= 10).

Figure S1

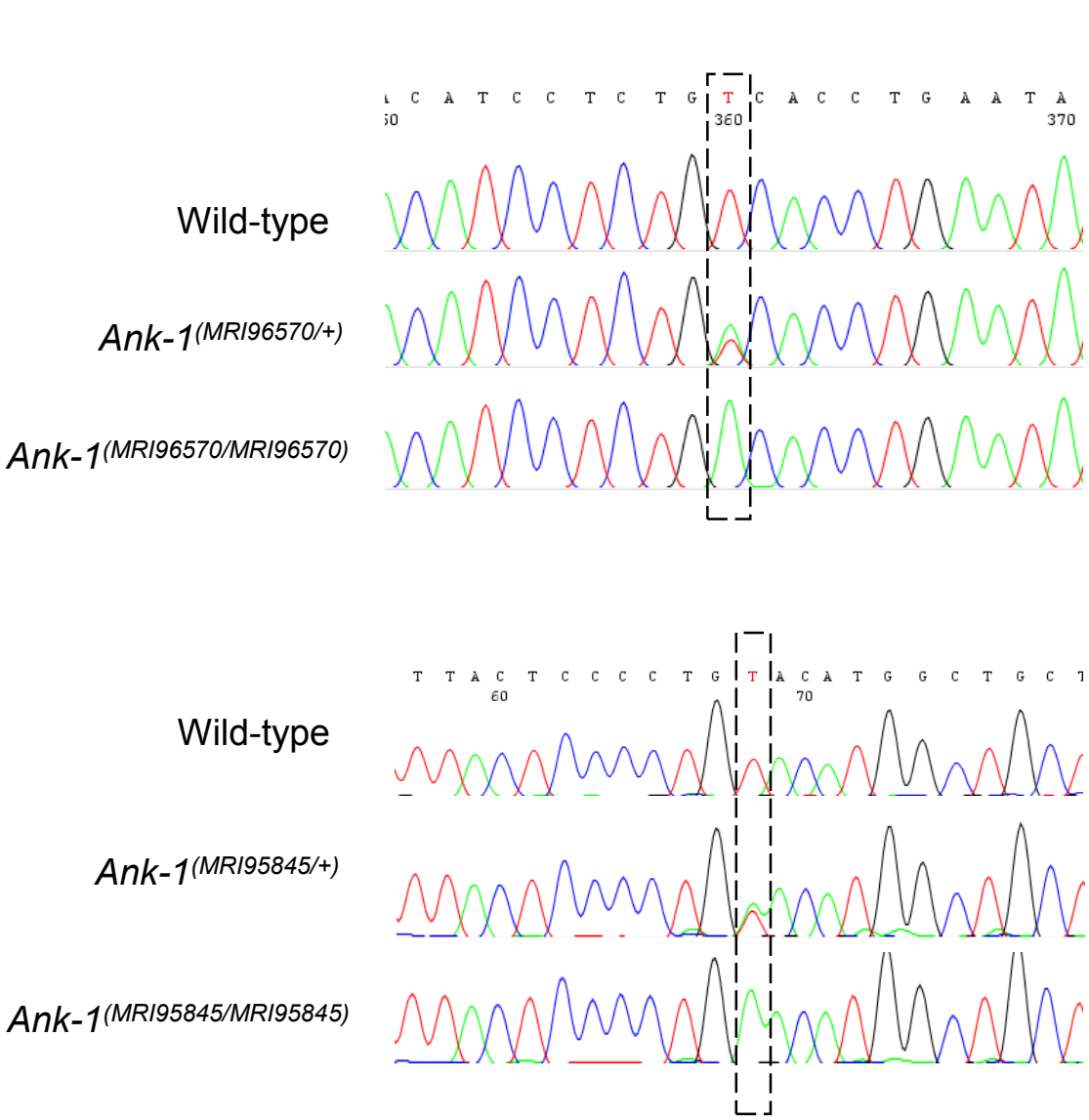

Figure S1. The location of *Ank-1*$^{(MRI96570)}$ and *Ank-1*$^{(MRI95845)}$ mutation. (A) Sanger sequencing of mice carrying *Ank-1*$^{(MRI96570)}$ revealed a T to A transversion in exon 34 of *Ank-1* gene, which is predicted to induce a premature stop codon. (B) Mice carrying *Ank-1*$^{(MRI95845)}$ mutation were found to have a T to A transversion in exon 5 of *Ank-1* gene, which is predicted to cause a missense mutation from tyrosine to asparagine at residue 149.

Table S2

Table S2. The complete blood count of *Ank-1*$^{(MRI96570/+)}$, *Ank-1*$^{(MRI95845/+)}$ and *Ank-1*$^{(MRI95845/MRI95845)}$ mice.

	Wild type	*Ank-1*$^{(MRI96570/+)}$	*Ank-1*$^{(MRI95845/+)}$	*Ank-1*$^{(MRI95845/MRI95845)}$
WBC (x10^6 /ml)	11.3±0.3	11.2±0.4	11.9±0.8	12.1±0.8
RBC (x10^9 /ml)	10.1±0.1	11.0±0.1***	10.7±0.1***	10.9±0.1***
HGB (g/L)	150.5±0.8	150.7±1.1	148.8±1.9	142.6±1.7*
MCV (fL)	52.3±0.2	46.9±0.2***	46.6±0.2***	43.0±0.1*** ^
MCH (pg)	14.9±0.1	13.7±0.1***	13.9±0.1***	13.1±0.2*** ^
MCHC (g/L)	285.3±1.2	290.3±1.8	298.3±2.4	294.7±4.0
RDW (%)	14.5±0.1	15.3±0.1***	16.1±0.3***	18.4±0.2*** ^
PLT (x10^6 /ml)	1036±31	1051±34	992±51	1026±53
Retics (%)	2.23±0.26	3.34±0.42	3.33±0.46	5.68±0.43***

The blood parameters were obtained from a haematological analyser ADVIA 120. WBC = white blood cell count; RBC = red blood cell count; HGB = total haemoglobin; MCV = mean corpuscular volume; MCH = mean corpuscular haemoglobin; MCHC = mean corpuscular haemoglobin concentration; RDW = red cell distribution width; PLT = platelet counts; Retics = percentage of reticulocytes, n=23-50. Bonferroni adjusted significance threshold = 0.001852, * P< 0.001, ** P< 1x10^{-5} compared to wild-type mice; whereas ^ P<0.001 compared to *Ank-1*$^{(MRI95845/+)}$ mice.

Figure S2

A)

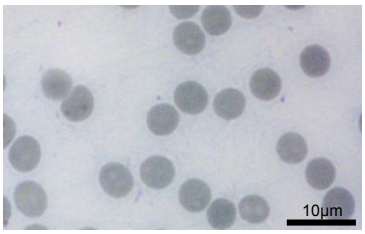

Wild-type

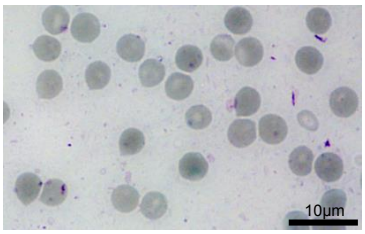

Ank-1$^{(MRI96570/+)}$

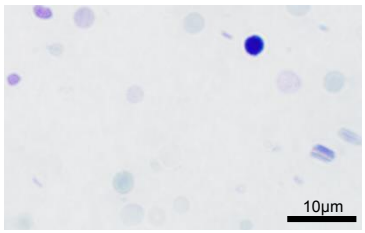

Ank-1$^{(MRI96570/MRI96570)}$

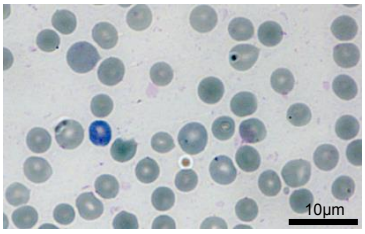

Ank-1$^{(MRI95845/+)}$

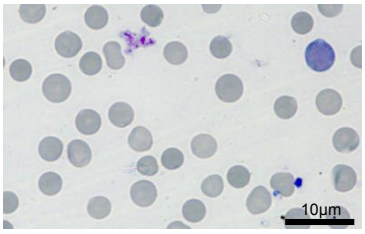

Ank-1$^{(MRI95845/MRI95845)}$

B)

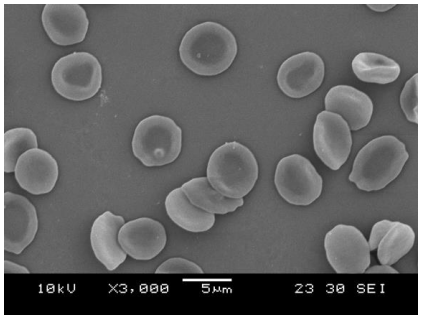

Wild-type

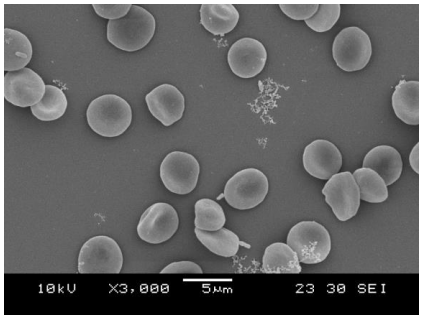

Ank-1$^{(MRI96570/+)}$

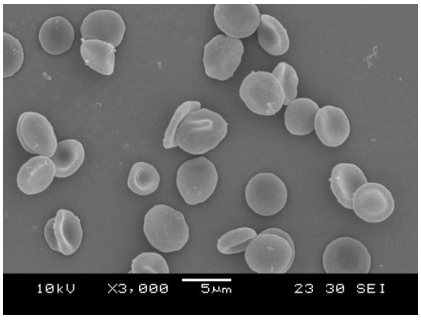

Ank-1$^{(MRI95845/+)}$

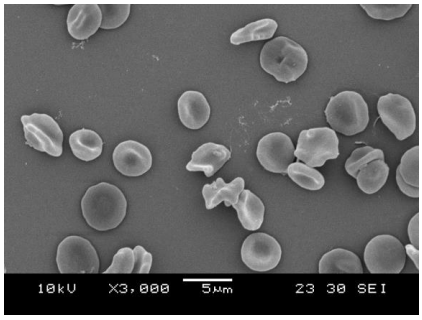

Ank-1$^{(MRI95845/MRI95845)}$

Figure S2. The RBC morphology of mice carrying *Ank-1*$^{(MRI96570)}$ or *Ank-1*$^{(MRI95845)}$ mutation. (A) Giemsa-stained blood smears as examined under light microscope at 1000x magnification. (B) Scanning electron microscopic images showing the RBC shape of *Ank-1*$^{(MRI96570/+)}$, *Ank-1*$^{(MRI95845/+)}$ and *Ank-1*$^{(MRI95845/MRI95845)}$ mice.

Figure S3

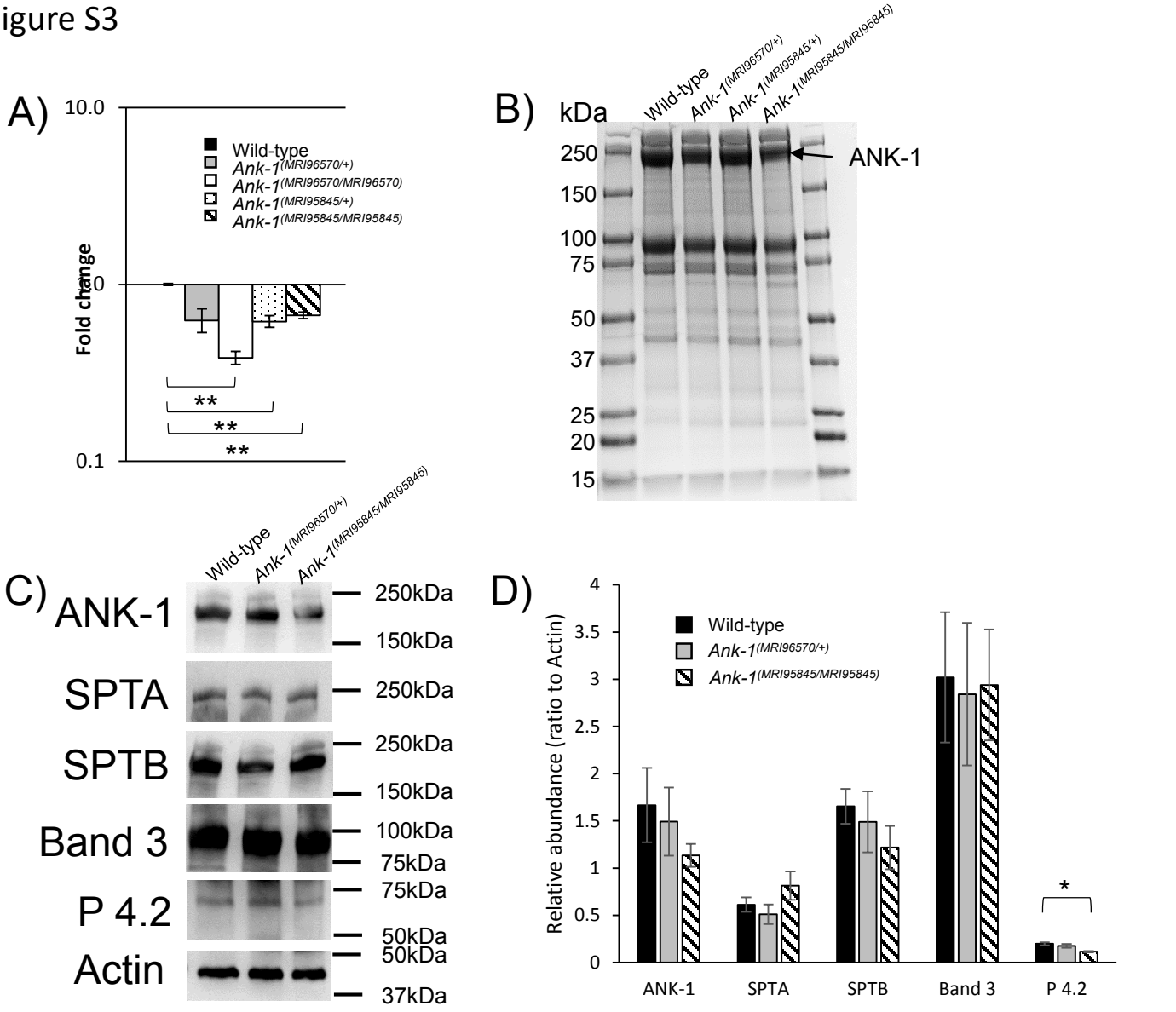

Figure S3. The expression of *Ank-1* and other RBC cytoskeletal proteins in mice carrying *Ank-1*$^{(MRI96570)}$ or *Ank-1*$^{(MRI95845)}$ mutation. (A) Quantitative PCR was carried out on E14 embryonic livers to examine *Ank-1* expression levels (n=3). The abundance of ANK-1 and other RBC cytoskeletal protein levels of *Ank-1*$^{(MRI96570/+)}$, *Ank-1*$^{(MRI95845/+)}$ and *Ank-1*$^{(MRI95845/MRI95845)}$ mice as examined via (B) Coomassie staining and (C) Western blotting on membrane of mature RBCs. (D) The relative abundance of various cytoskeletal protein levels calculated from western blots (n=3). SPTA = α-spectrin, SPTB = β-spectrin, P 4.2 = Protein 4.2. * $P<0.05$, ** $P<0.01$. Error bars indicate SEM.

Figure S4

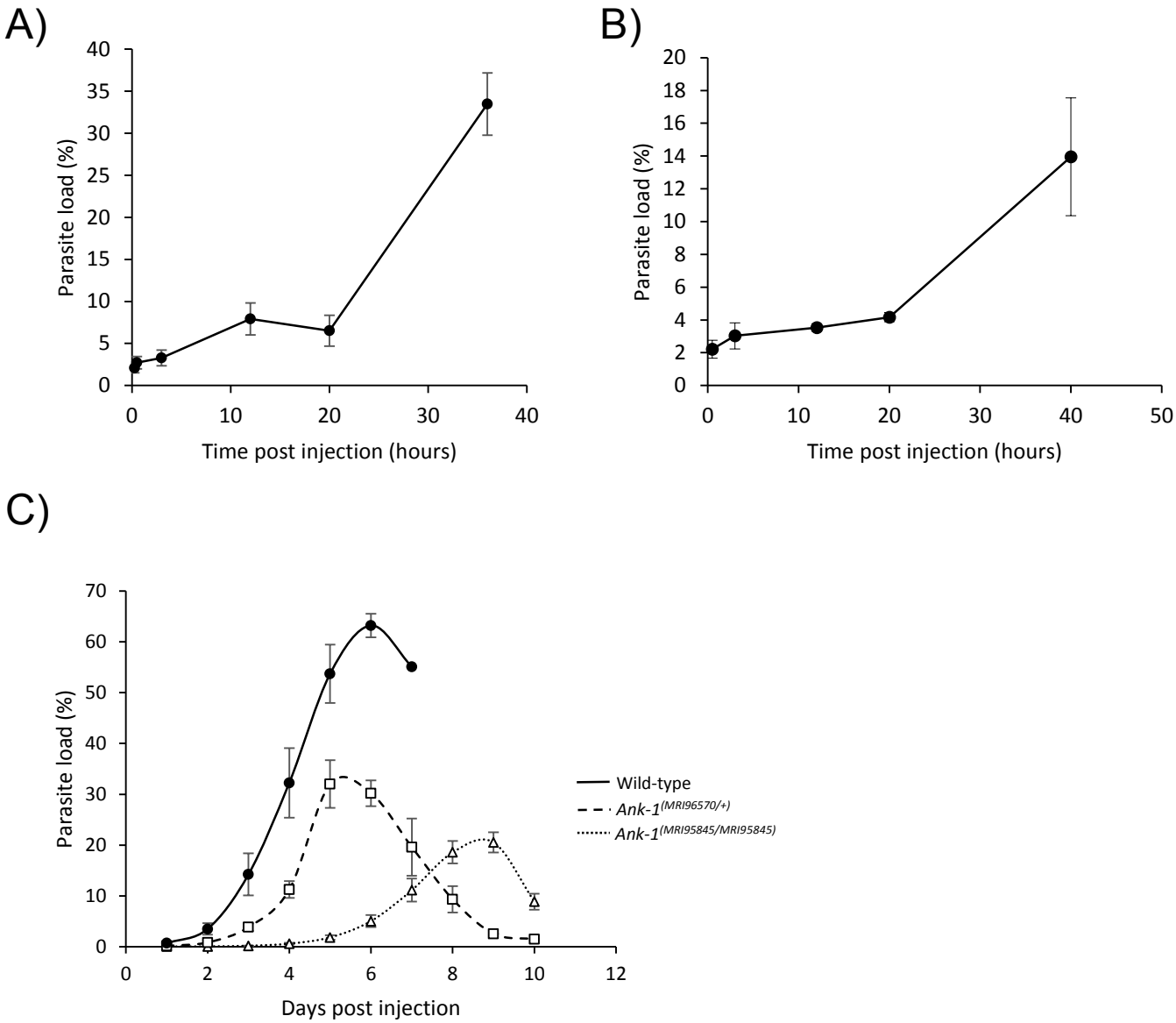

Figure S4. The parasitemia of the host mice during IVET assays and half-life assay. The parasitemia curve of the host mice during IVET assays, when comparing (A) wild-type with *Ank-1*$^{(MRI95845/MRI95845)}$ erythrocytes, and (B) *Ank-1*$^{(MRI96570/+)}$ with *Ank-1*$^{(MRI95845/MRI95845)}$ erythrocytes (n=5-7). (C) The parasitemia curve of wild-type, *Ank-1*$^{(MRI96570/+)}$ and *Ank-1*$^{(MRI95845/MRI95845)}$ mice during RBC half-life assay (n=6-7).